



117
310
THS

MICHIGAN STATE UNIVERSITY LIBRARIES



3 1293 00881 2608

This is to certify that the
thesis entitled

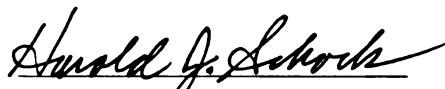
EXPERIMENTAL INVESTIGATION OF THE FLOW FIELD
IN AN AUTOMOTIVE TORQUE CONVERTER

presented by

DANIEL WARREN MCCARRICK

has been accepted towards fulfillment
of the requirements for

MASTERS degree in MECHANICAL ENGINEERING


Major professor

Date 7/30/93

LIBRARY Michigan State University

PLACE IN RETURN BOX to remove this checkout from your record.
TO AVOID FINES return on or before date due.

DATE DUE	DATE DUE	DATE DUE
SEP 26 1997		
FEB 10 1995		
MAY 29 1995		
MAY 29 1995		
FEB 2 1998		

MSU Is An Affirmative Action/Equal Opportunity Institution

c:\circ\datedue.pm3-p.1

**EXPERIMENTAL INVESTIGATION OF THE FLOW FIELD IN AN
AUTOMOTIVE TORQUE CONVERTER**

By

Daniel Warren McCarrick

A THESIS

**Submitted to
Michigan State University
in partial fulfillment of the requirements
for the degree of**

MASTER OF SCIENCE

Department of Mechanical Engineering

1993

ABSTRACT

EXPERIMENTAL INVESTIGATION OF THE FLOW FIELD IN AN AUTOMOTIVE TORQUE CONVERTER

By

Daniel Warren McCarrick

The internal flow field in an automotive torque converter is highly complex and has yet to be studied in depth. The goal of this study was to determine the feasibility of using Laser Doppler Velocimetry (LDV) to quantify the internal flow in a torque converter.

An impeller passage of a Ford prototype torque converter was fitted with a window and test equipment designed to permit optical access to the passage. Data was collected at two speeds and four speed ratios. In the middle of the passage the flow was not influenced by the instantaneous position of the turbine blades. Flow rates and turbulence levels were found to be inversely proportional to the speed ratio. The passing of the turbine blades did affect the flow in the gap region between the impeller and turbine. A flow animation of the velocity measurements revealed evidence of a secondary flow in the gap region.

ACKNOWLEDGMENTS

I would like to take this opportunity to thank those people without whose help this study would not have been possible. First, my major professor Dr. Harold Schock for his time and assistance in making this project a reality; to Tom Stuecken, Roy Schafer, Tim Fitzpatrick, John Kuchar, and Scott Sober for their help in designing, building and testing the experimental equipment; to Dr. Keunchul Lee and Seoung-Chool Yoo for their assistance with the LDV system and computer programming; to Dr. Craig Somerton for his knowledge and advice on numerous matters; and to Mark Novak whose knowledge of PV~WAVE made the animation of the flow possible.

I would also like to express my gratitude to Mr. George Lee and the Ford Motor Company for their financial support.

Finally I would like to thank my wife, Maria, for her patience and support during my graduate studies.

TABLE OF CONTENTS

	Page
LIST OF TABLES	vi
LIST OF FIGURES	vii
NOMENCLATURE	x
CHAPTER 1- INTRODUCTION	1
1.1 Torque Converter Fundamentals	1
1.2 Problem Statement	3
1.3 Literature Review	3
CHAPTER 2 - EXPERIMENTAL EQUIPMENT	6
2.1 Torque Converter	6
2.2 Torque Converter Test Stand	6
2.3 Torque Converter Fixture	10
2.4 Laser Doppler Velocimetry System	12
CHAPTER 3 - PRELIMINARY TESTING	16
3.1 Window Insert Material	16
3.2 Transmission Oil	18
3.3 Test Stand Limitations	20
3.4 Seeding Experiments	21
CHAPTER 4 - EXPERIMENTAL PROCEDURE	24
4.1 Data Acquisition Checklist	24
4.2 Rotary Shaft Encoder References	24
4.3 Traverse Table Reference	26
4.4 LDV Signal Check	27
4.5 Speed Control of the Impeller and Turbine	28
4.6 Frequency Shift Magnitude and Direction	28
4.7 Data Acquisition Software Configuration	29
4.8 Data Acquisition	30

	Page
4.9 Test Envelope Development	31
CHAPTER 5 - DATA PROCESSING AND DISPLAY	34
5.1 TSI Software Limitations	34
5.2 Format of Initial Velocity Data	34
5.3 Velocity Data Conversion	35
CHAPTER 6 - RESULTS AND DISCUSSION	38
6.1 Phase One Results	38
6.2 Phase Two Results	45
CHAPTER 7 - SUMMARY AND CONCLUSIONS	70
CHAPTER 8 - RECOMMENDATIONS	72
LIST OF REFERENCES	73

LIST OF TABLES

	Page
Table 1. Torque converter specifications	6
Table 2. Transmission oil properties	19
Table 3. Converter efficiency as a function of speed ratio	20
Table 4. Properties of seeding particles tested	21
Table 5. Basic TSI phase software inputs	30
Table 6. Measurement envelope for the first phase of testing	38
Table 7. Measurement envelope for the second phase of testing	45

LIST OF FIGURES

	Page
Figure 1. Torque converter assembly	1
Figure 2. Torque converter test stand	7
Figure 3. LDV system with torque converter test stand	8
Figure 4. 50 Hp drive and dynamometer with belt and pulley	
drive system	8
Figure 5. Oil conditioning cart.....	9
Figure 6. Schematic of torque converter oil supply system	9
Figure 7. Schematic of torque converter fixture bearing	
lubrication system	10
Figure 8. Torque converter with its bracket and fixture	11
Figure 9. Torque converter bracket and fixture mounted on test stand	11
Figure 10. Schematic of the Laser Doppler Velocimetry System	13
Figure 11. Plexiglas window insert	17
Figure 12. Plexiglas window insert installed in the impeller	17
Figure 13. Light transmission characteristics of Plexiglas	18
Figure 14. Transmission characteristics of oil samples	19
Figure 15. Position of impeller and turbine at their zero	
degree encoder references	25
Figure 16. Traverse table coordinate system	26
Figure 17. Off-axis back scatter configuration	32

	Page
Figure 18. Illustration of relative impeller and turbine blade position after rotation	36
Figure 19. Y velocity components at 1000 rpm and no-load speed ratio ...	40
Figure 20. Y velocity components at 1000 rpm and 0.50 speed ratio	40
Figure 21. Y velocity components at 1000 rpm and 0.25 speed ratio	41
Figure 22. X velocity components at 1000 rpm and no-load speed ratio ...	41
Figure 23. X velocity components at 1000 rpm and 0.50 speed ratio	42
Figure 24. X velocity components at 1000 rpm and 0.25 speed ratio	42
Figure 25. Standard deviations of X velocities independent of turbine angle	44
Figure 26. Standard deviations of Y velocities independent of turbine angle	44
Figure 27. X velocity components 2 mm from turbine entrance, 0.50 speed ratio	46
Figure 28. X velocity components 1 mm from turbine entrance, 0.50 speed ratio	46
Figure 29. X velocity components at the turbine entrance plane, 0.50 speed ratio	47
Figure 30. Y velocity components 2 mm from turbine entrance, 0.50 speed ratio	48
Figure 31. Y velocity components 1 mm from turbine entrance, 0.50 speed ratio	48
Figure 32. Y velocity components at the turbine entrance plane, 0.50 speed ratio	49
Figure 33. X velocity components at the turbine entrance, 0.75 speed ratio	50

	Page
Figure 34. X velocity components at the turbine entrance plane, 0.25 speed ratio	50
Figure 35. X velocity standard deviations at turbine entrance, 0.75 speed ratio	51
Figure 36. X velocity standard deviations at turbine entrance, 0.50 speed ratio	51
Figure 37. X velocity standard deviations at turbine entrance, 0.25 speed ratio	52
Figure 38. X velocity vectors at 1000 rpm, 110 mm radius, and a 0.50 speed ratio	56
Figure 39. X and Y resultant velocity vectors at turbine entrance	63

NOMENCLATURE

d_f	Fringe spacing
d_p	Diameter of the seeding particle
f	Frequency response of the particle
F_d	Doppler frequency
L_c	Characteristic length of the system
St	Stokes number
U_c	Characteristic velocity of system
V	Velocity of particle as determined by Doppler frequency
κ	Half angle between laser beams
λ	Wavelength of laser light
μ	Dynamic viscosity of the transmission oil
ρ_p	Density of the seeding particle
τ	Particle relaxation time

CHAPTER 1

INTRODUCTION

1.1 Torque Converter Fundamentals

A torque converter is a hydrodynamic device used to transfer power smoothly from the engine to the transmission of an automobile. A typical torque converter assembly is shown in Figure 1.

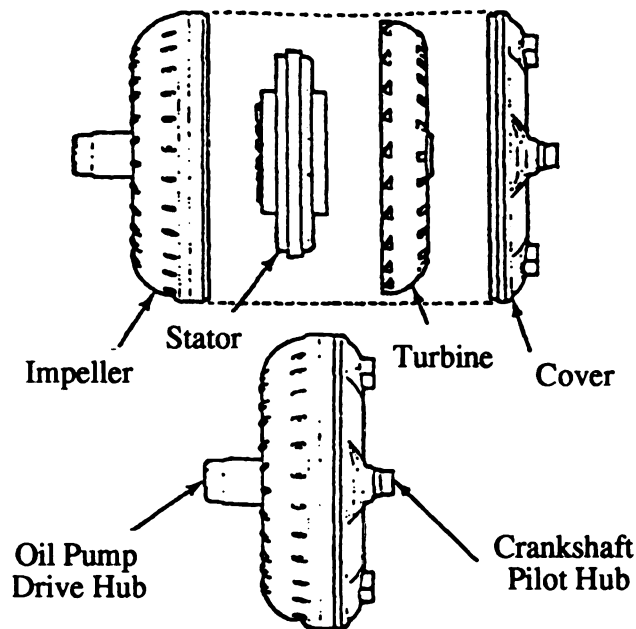


Figure 1. Torque converter assembly

The assembly consists of three working elements that operate within a fluid circuit. A pump, also called an impeller, is attached directly to a cover and then to the flexplate of the engine and always rotates at the same speed as the engine. The impeller consists of a housing and blades that form passages that direct the working fluid, transmission oil, towards the turbine. The turbine sits freely inside

the cover and is attached directly to the transmission shaft and contains similar blades and passages that are curved in the opposite direction to those of the impeller. The turbine is driven by the fluid pumped by the impeller. The stator is used to redirect the flow from the turbine back into the impeller. A basic converter operational scenario might consist of the following. When an automobile is at a standstill with the brakes applied, the impeller is rotating at the engine idle speed; and the turbine and transmission shaft are held stationary. When the brakes are released and the accelerator depressed, impeller speed increases; and the turbine is now free to rotate. The impeller rotation causes transmission oil to be pumped through the passages and into the turbine. The fluid causes the turbine, and therefore the transmission shaft to rotate. The ratio of turbine speed to pump speed is known as the speed ratio. The stator redirects the fluid as it exits the turbine passages and reenters the impeller. If the stator was not present to redirect the flow, the momentum of the fluid would create a force acting against the rotation of the impeller instead of assisting it. A one-way clutch prevents the stator from rotating with the impeller and turbine. Once the turbine has reached approximately 90 percent of the speed of the impeller, the one-way clutch unlocks and the three elements are allowed to turn together. This is known as the coupling point. In some converters a direct mechanical linkage is established between the impeller and turbine at the coupling point, thereby eliminating the fluid coupling. This is known as converter lock-up. This condition will remain until something causes a speed change in the engine that will terminate the lock-up phase and reestablish the fluid coupling [1].

The fluid flow inside the converter is extremely hard to visualize due to its complex nature and highly three-dimensional geometry. Current flow simulations have not been developed to the point where design from theoretical results can be relied upon. Accurate measurements are needed to help build and verify effective

models that can be used in the design process. The efficiency of the torque converter can be greatly enhanced by optimizing the internal flow paths. Increased efficiency will lead to greater fuel economy, always an important consideration in the design of an automobile. Examining the effect of various torque converter sizes and shapes is also important, especially when considering the space limitations of front-wheel drive vehicles.

1.2 Problem Statement

The objective of this study is to determine the feasibility of using LDV on an operational torque converter and to develop a subsequent experimental procedure. The most difficult obstacle in developing such a method is achieving optical access to the internal flow in the torque converter. This requires that the test stand and supporting equipment be as compact as possible and a window be placed in a torque converter without significantly altering its flow characteristics. This method can be then used to quantify the flow field in the converter. The results can be compared to theoretical data from current models and help improve them. An animation of the data can also be used to better understand the physical characteristics of the flow in the converter.

1.3 Literature Review

In 1988 By and Mahoney [2] outlined the technology needs for the automotive torque converter. The emergence of various laser anemometry techniques over the last few decades has given scientists a non-intrusive method of measuring velocities in closed systems. Experimental research has been conducted on several types of turbomachines such as axial flow compressors and

pumps [3-5]. However, quantitative velocity measurements in an automotive torque converter have been extremely limited to date.

Fister and Adrian [6] were the first to measure the flow field in a converter and examine the relationship between the three elements. They used two geometrically identical converters. One converter used water as the working fluid and a Laser-Two-Focus method (L2F) to measure flow velocity. The other converter used air as the working fluid and a spark-tracer method to measure velocity. Pressure measurements were also made using multi-holed ports in the gap region between the elements. This study has some limitations in its usefulness. The most obvious is that the working fluid was not transmission oil. Also the converters used were not automotive, but larger industrial units which allowed for easier measurements.

Bahr et al. [7] have published the most extensive internal torque converter flow data so far. They used a Laser Doppler Velocimetry (LDV) system to map the velocity field in the stator of a torque converter. They used a torque converter constructed entirely of Plexiglas to allow for optical access to the stator. The entire converter was placed in a containment box filled with oil to reduce the effect of refractive index differences. A clear transmission oil was seeded with 4 micron aluminum oxide particles to obtain a Doppler signal. A total of five planes were examined, one each at the inlet and exit planes of the stator and three in between. Twenty five positions in each plane and 2000 data points for each position were measured. All three velocity components for each position were measured, one component at a time. Rotary shaft encoders were used to record the instantaneous position of the impeller and turbine. Measurements were taken at two different speed ratios; 0.80 at 1100 rpm and 0.065 at 800 rpm. The flow was found to be moderately turbulent. Flow rates and torque distributions were found to vary significantly from one-dimensional flow theory. The angle of entrance into the

stator had a significant effect on flow separation, especially at off-design speed ratios. A surprising finding was that the instantaneous position of the impeller and turbine did not noticeably affect the flow field in the stator. The major limitation of this study was in the fabrication of the torque converter. A Plexiglas torque converter may not accurately represent the behavior of an operational converter, especially at higher speeds and increased loads. Also, no mention was made about any attempt to make measurements in other areas of the converter.

Numazawa et al. [8] developed a flow visualization technique to trace flow patterns on the blade, core, and shell surfaces of the three converter elements. The technique involves placing epoxy-like dots on the internal passages of a torque converter. As the transmission oil is heated, the dots begin to streak to form flow patterns. A similar method has recently been developed and used by Yang at the University of Michigan as a companion project to this study. Both studies yield useful information about the presence of swirl, separated flow, and flow reversal. However, these methods do not provide quantitative velocity data or information on the flow in the region between the blades.

A limitation recognized at the onset of this study was that the LDV system used at the Michigan State University Engine Research Laboratory (MSUERL) can only measure two velocity components in its current configuration. The system can be upgraded to measure all three velocity components, but at a significant cost. Before such an investment is considered, the validity of the method must be established.

CHAPTER 2

EXPERIMENTAL EQUIPMENT

2.1 Torque Converter

A Ford Motor Company prototype torque converter was modified for use in this study. The converter cover was cut in half to separate the impeller and turbine. Threaded flanges were welded to the impeller housing and the remaining part of the cover. This allowed the converter to be taken apart, altered as necessary, and reassembled. Table 1 lists some specifications of the converter.

Table 1. Torque converter specifications

Diameter	267 mm
Axial Length	95.3 mm
Number of Impeller Passages	31
Number of Turbine Passages	27

2.2 Torque Converter Test Stand

The torque converter test stand consists of a 50-Hp dc drive, a 50-Hp universal dynamometer, oil conditioning unit, bedplate assembly, and fixture bracket. The drive and dynamometer are placed on the bedplate below the fixture bracket to allow for maximum optical access to the converter. The 50-Hp dc drive and the 50-Hp Universal Dynamometer are used to simulate an automotive engine and road loads, respectively. Both the drive and dynamometer use a system of

belts and pulleys as a drive mechanism. The dc drive can produce 2500 rpm, and the pulley system is geared to drive the converter at 5000 rpm. The dynamometer is geared in a one-to-one fashion and can rotate at 5000 rpm. The speed of the dc drive and dynamometer are independently regulated via separate controllers. Safety guards surround the belt and pulley systems in case of component failure. Figures 2,3, and 4 are photographs of the test stand.

An oil conditioning cart contains the oil supply system for the converter and a lubrication system for the fixture bearings. A water-cooled heat exchanger is included in the oil supply system to cool the oil after it returns from the converter. The temperature of the transmission oil before it enters and immediately after it exits the converter is monitored using two type T thermocouples in combination with an Omega DP80 Series monitor. A photograph of the oil conditioning cart is shown in Figure 5 and schematics for the oil supply and lubrication systems are shown in Figures 6 and 7.

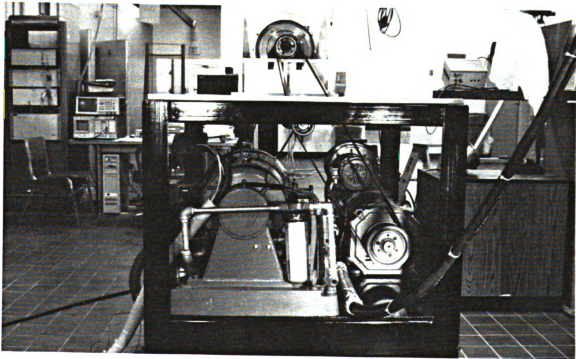


Figure 2. Torque converter test stand

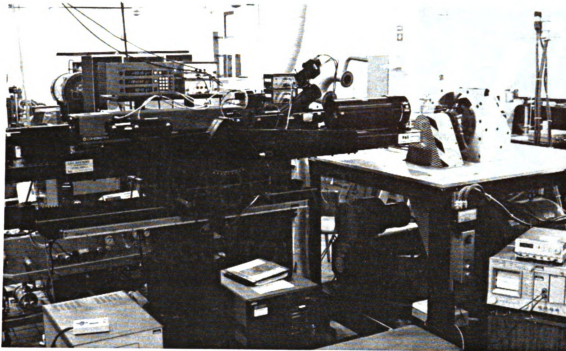


Figure 3. LDV system with torque converter test stand

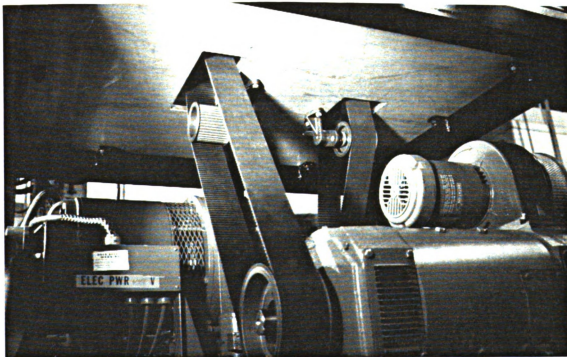


Figure 4. 50 Hp drive and dynamometer with belt and pulley drive system

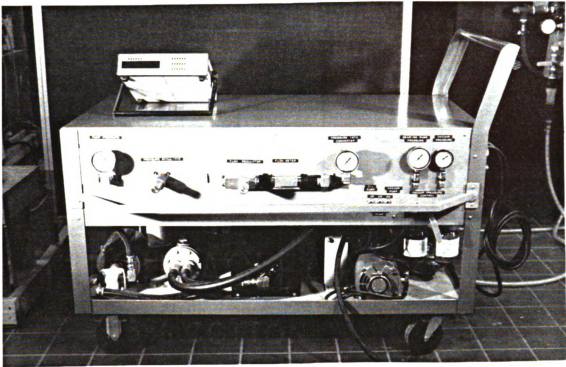


Figure 5. Oil conditioning cart

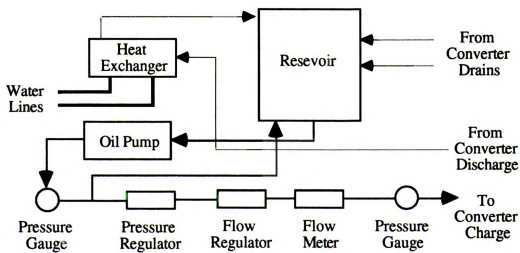


Figure 6. Schematic of torque converter oil supply system

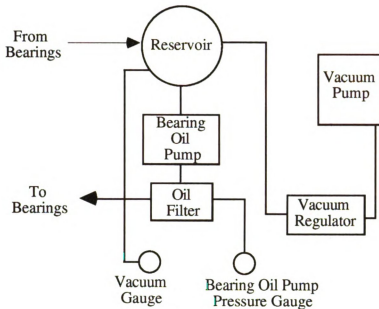


Figure 7. Schematic of torque converter fixture bearing lubrication system

2.3 Torque Converter Fixture

In order to make successful LDV measurements in any device, the region of interest must be accessible to the focused laser beams. This was the most important consideration in the design of the torque converter fixture. The fixture is constructed as compact as possible to ensure optical access to both the impeller and turbine sides. Rotary shaft encoders are mounted directly below the impeller and turbine bearings. The shaft encoders are driven by a belt and pulley system that connects the bearings to the encoders. The torque converter fixture is attached to the fixture bracket. The fixture bracket is mounted on the bedplate assembly and supports the converter and the fixture. The fixture bracket was also designed to allow optical access to the converter. Figures 8 and 9 are photographs of the fixture.

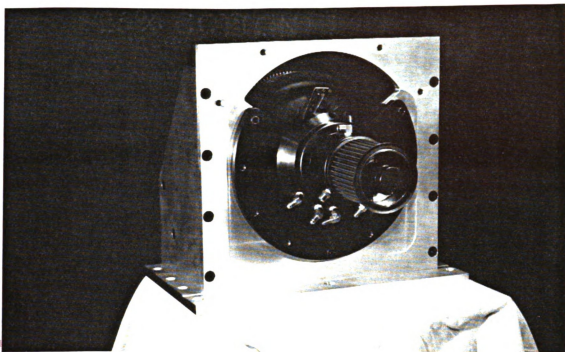


Figure 8. Torque converter with its bracket and fixture

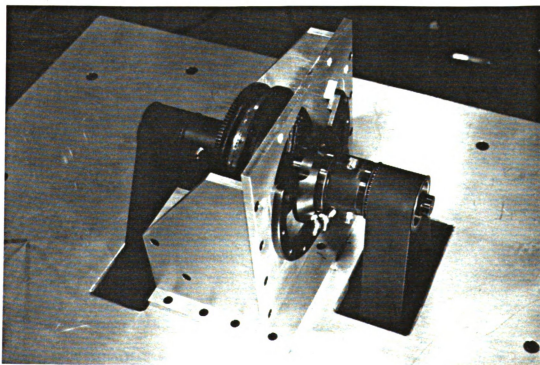
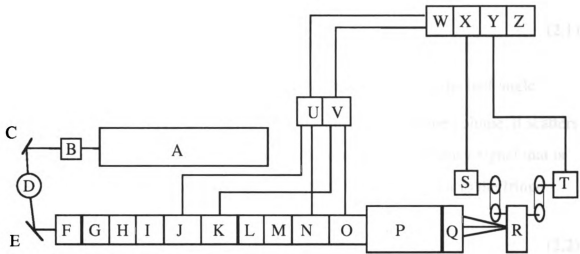


Figure 9. Torque converter bracket and fixture mounted on test stand

2.4 Laser Doppler Velocimetry System

The Laser Doppler Velocimetry system consists of a four-watt argon-ion laser manufactured by Coherent, optical and signal processing equipment built by TSI, Inc., and an IBM PS/2 80 computer for data acquisition. The system is currently capable of measuring two velocity components simultaneously. A schematic of the LDV system is shown in Figure 10. The laser and optics are mounted on a TSI model 9900-1 traverse table. This method allows for great flexibility and accuracy in positioning the measurement volume within the torque converter. Translation in three directions is achieved by using a hand-held controller. A digital readout of position is provided by a Sony Magnascale LM 22 indicator.

The LDV system operates as follows. The alphabetical references apply to Figure 10. The laser (A) produces a beam of light that is directed into a beam collimator (B). A steering mirror (C) directs the beam of light into a prism (D), which separates the light into distinct wavelengths. Two wavelengths, 488.0 nm and 514.5 nm, are selected and directed into the optical path of the system by another steering mirror (E). Each of the beams is split into two beams of equal intensity by beam splitters (F and G). One beam from each wavelength is passed into separate Bragg cells (J and K). The other beams are passed through wedge compensators to assure that all beams travel equal optical path lengths. The additional beams created by the Bragg cells are blocked by the beam stop (L). A beam spacer (M) is used to properly space the beams for use by the beam expander (P). The beams are then focused to an intersection point known as the probe measuring volume by a focusing lens (Q). When two coherent beams intersect, an interference pattern of equally spaced fringes is formed. The spacing of the fringes is a function of the wavelength of the



- | | |
|-----------------------------|---------------------------------|
| A) ARGON-ION LASER | N) RECEIVING OPTICS - 488.0 nm |
| B) BEAM COLLIMATOR | O) RECEIVING OPTICS - 514.5 nm |
| C) STEERING MIRROR | P) BEAM EXPANDER |
| D) PRISM | Q) FOCUSING LENS |
| E) STEERING MIRROR | R) TORQUE CONVERTER |
| F) BEAM SPLITTER - 488.0 nm | S) IMPELLER SHAFT ENCODER |
| G) BEAM SPLITTER - 514.5 nm | T) TURBINE SHAFT ENCODER |
| H) POLARIZER - 488.0 nm | U) FREQUENCY SHIFTER - 488.0 nm |
| I) POLARIZER - 514.5 nm | V) FREQUENCY SHIFTER - 514.5 nm |
| J) BRAGG CELL - 488.0 nm | W) IFA 750 SIGNAL PROCESSOR |
| K) BRAGG CELL - 514.5 nm | X) ROTATING MACHINE RESOLVER |
| L) BEAM STOP | Y) ROTATING MACHINE RESOLVER |
| M) BEAM SPACER | Z) MASTER INTERFACE UNIT |

Figure 10. Schematic of the Laser Doppler Velocimetry System

beam and the angle between the beams given by the equation

$$d_f = \frac{\lambda}{2 \sin \kappa} \quad (2.1)$$

where d_f is the fringe spacing, λ is the wavelength, and κ is the half angle between the beams. As a seed particle passes through the probe volume, it scatters light at different intensities. This produces an oscillating frequency signal that is directly related to the velocity component which is perpendicular to the fringe pattern by the equation

$$V = d_f \times F_d \quad (2.2)$$

where V is the velocity, and F_d is the Doppler frequency of the scattered signal. The fringe patterns that are formed would normally be stationary. This means that a particle traveling at the same speed in either direction in relation to the fringe pattern would produce the same frequency and hence the same velocity. This would make it impossible to determine the direction of the flow. The function of the Bragg cell is to move the pattern in a desired direction at a known frequency so that the direction of the flow can be determined. The scattered light from the particles is collected by the receiving optics (N and O) and focused on separate photomultipliers for each wavelength of light.

It is important to note that these receiving optics can be positioned anywhere, as long as they receive the scattered light. Ideally, the receiving optics should be positioned on the far side of the probe volume, relative to the laser. This is known as forward scatter. The opposite of this configuration is known as back scatter, when the receiving optics are placed on the near side of the probe volume. In general, it is preferable to use forward scatter over back scatter when ever possible since the intensity of the scattered light can be 100 to 1000 times greater in the forward scatter direction [9]. There are two types of back scatter

configurations, on-axis and off-axis. On-axis back scatter refers to the situation when the receiving optics are placed in the same optical path over which the original laser beams were sent and uses the same lenses to collect and focus the light on the photomultipliers. Off-axis back scatter refers to the situation where the receiving optics are placed outside of the optical path of the laser beams and use their own lenses to collect and focus the scattered light. Off-axis is generally a simpler configuration to use since the receiving optics are out of the plane of the laser beams and the probe volume is easier to locate and focus on. The receiving optics in Figure 10 are shown in on-axis back scatter.

The photomultipliers produce frequency signals that are proportional to the velocities. The signals are then sent to the frequency shifters (U and V). The frequency shifter allows the adjustment of the zero velocity reference frequency. The signal is then sent to the TSI IFA 750 Signal Processor (V) where the velocity is calculated. At the same time velocity data is being taken and processed, information from both rotary shaft encoders is sent to the corresponding rotating machine resolver (X and Y). These encoders produce 1024 evenly spaced pulses per revolution. This resolution can be increased by a factor of two or four through software manipulation. This arrangement allows all velocity data to be stamped with the instantaneous rotational position of both the impeller and turbine.

CHAPTER 3

PRELIMINARY TESTING

3.1 Window Insert Material

In order to allow access of the laser beams to the passages of the converter, a window insert was fabricated. The perfect window material should be simple and inexpensive to machine, able to be polished, transmit light at the proper frequencies, not react with transmission oil, and withstand temperatures up to 300 °F. Finding a material that met these criteria was difficult. Quartz satisfied the optical and temperature criteria, but would be difficult and expensive to machine. The maximum temperature Plexiglas can withstand before starting to deform is approximately 160°F. This deficiency was determined to be acceptable since Plexiglas met all the other requirements and could be fabricated much faster than a Quartz window. The index of refraction of Plexiglas is 1.490. Figure 11 is a photograph of the window and Figure 12 shows the window installed in the impeller housing. A Varian Cary1E spectrophotometer was used to confirm that Plexiglas transmitted light at frequencies between 400 and 550 nm, which covers the operating range of the LDV system. Figure 13 shows the results of the test. Plexiglas transmits over 90 percent of the light at the frequencies of interest, 488.0 and 514.5 nm, and meets the criteria. A decision was made to place the window in the impeller housing because that location was the most optically accessible to the LDV system. The window was formed by removing all the blades from an impeller section. A section of housing was removed and a piece of Plexiglas inserted. The Plexiglas material inside the housing was machined away so that the window would follow the contour of the housing. This window was then inserted

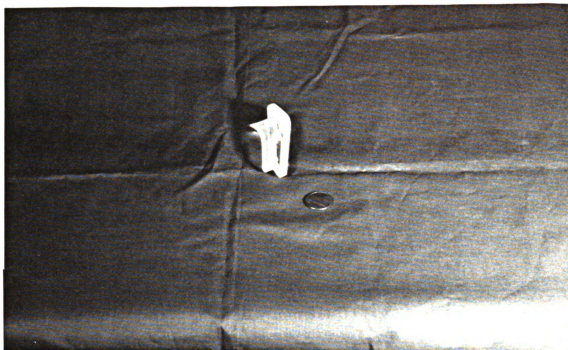


Figure 11. Plexiglas window insert



Figure 12. Plexiglas window insert installed in the impeller

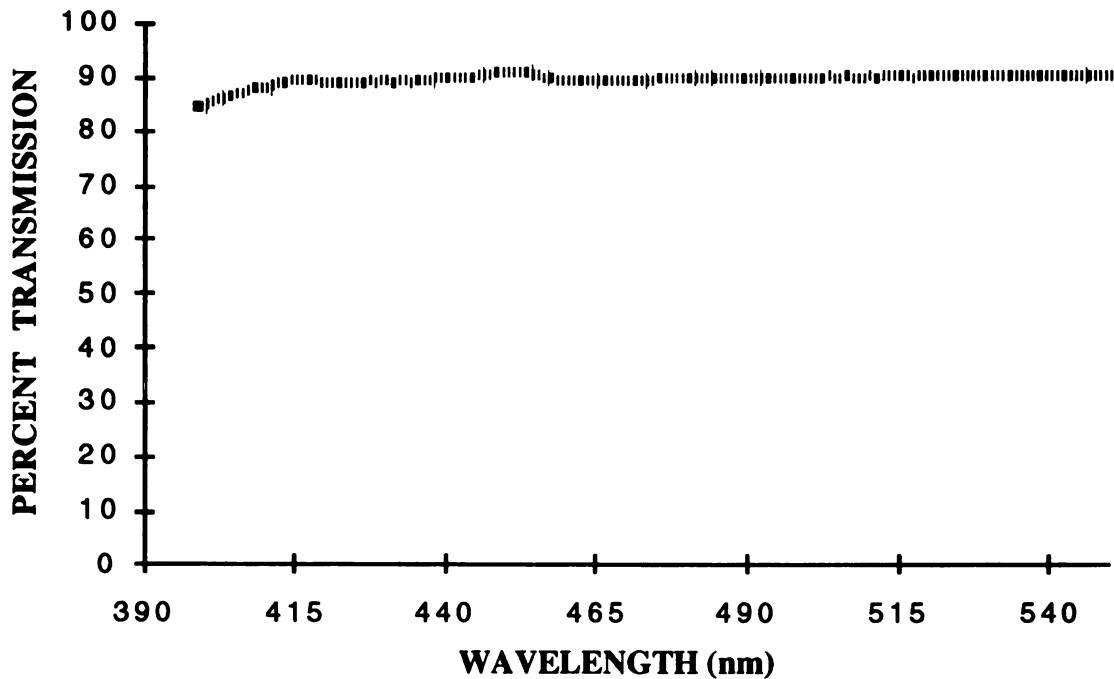


Figure 13. Light transmission characteristics of Plexiglas

in another impeller section with an identical section of housing removed. Finally the window was polished, sealed, and fastened to the impeller housing.

3.2 Transmission Oil

The most important characteristic of the transmission oil used in the converter assembly is its ability to transmit light at the appropriate wavelengths. Three samples of transmission oil were obtained from Exxon. One sample was the clear base stock oil that is used in the production oil; another sample was an undyed production oil with a slight red tint; and the last sample was the actual production oil that had a deeper red tint. A spectrophotometer test was conducted to determine the transmission characteristics of the three samples. Figure 14

shows the results of the test. The data for the production oil was omitted because the transmission was essentially zero at all frequencies and obscured the chart when plotted. Obviously the clear base stock oil has the best transmission properties and was chosen for use in the converter. Properties of the base stock oil are given in Table 2. The refractive indices of Plexiglas and the transmission oil are nearly identical. This eliminates any optical problems associated with making LDV measurements in closed systems with curved surfaces.

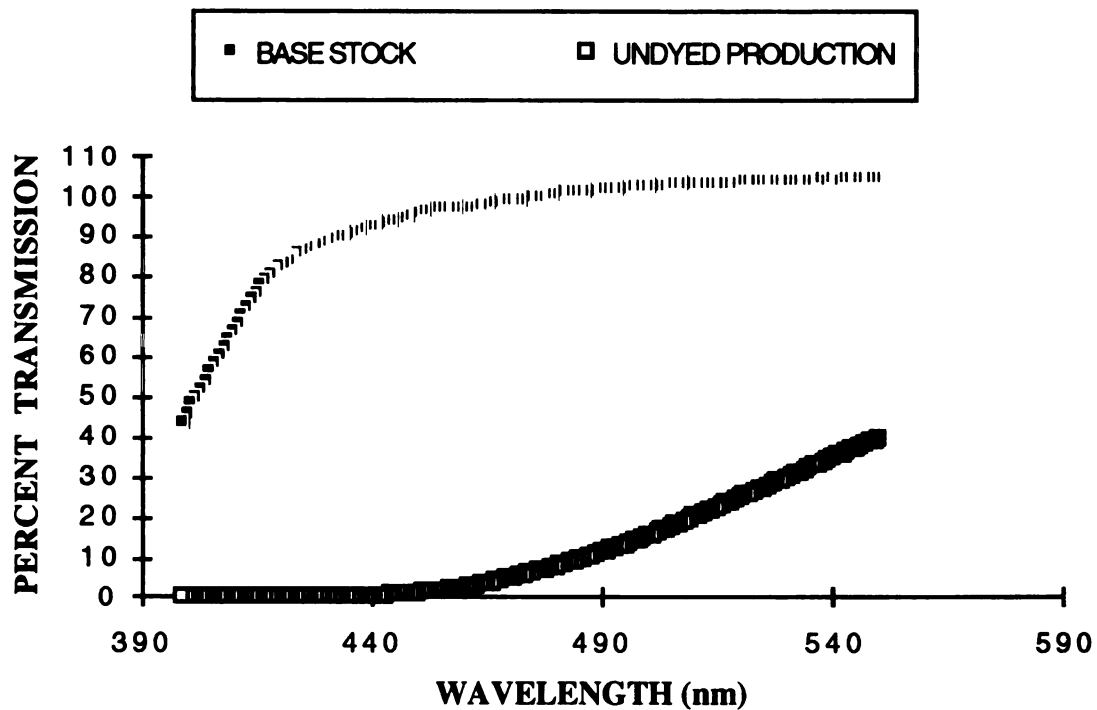


Figure 14. Transmission characteristics of oil samples

Table 2. Transmission oil properties

Density	$860 \text{ Kg} / \text{m}^3$
Dynamic Viscosity	$18.66 \times 10^{-3} \text{ Kg} / \text{ms}$
Index of Refraction	1.457

3.3 Test Stand Limitations

The operating limits of the experimental equipment were tested using an unmodified torque converter. The goal was to determine the envelope of conditions that could be simulated with the test stand. Items examined included the maximum converter speed and subsequent speed ratios that could be attained and any subsequent heating or noise problems. The tests revealed 3600 rpm at a no-load speed ratio to be the practical limit of the test stand. The no-load speed ratio is as close to a one-to-one speed ratio as can produced by the system. The only load incurred by the converter is due to friction. When an additional load is applied to the converter at this speed to induce a speed ratio, the 50-Hp drive is overloaded and automatically shuts down. Noise also became a significant problem at this speed. Insulation of the test stand will be required in order to test higher speeds. A combination of converter speed above 1500 rpm and speed ratios on the order of 0.25 produced significant heating problems. The temperature of the oil rapidly approaches the 160 °F limit of the Plexiglas. The problem is not in the capability of the heat exchanger in the oil conditioning cart to remove heat, but in the fact that much of the energy from the drive goes into heating the oil due to the inefficiency of the converter under these operating conditions. Table 3 is a chart showing the relationship between speed ratio and efficiency of the converter [10].

Table 3. Converter efficiency as a function of speed ratio

Speed Ratio	Efficiency	Speed Ratio	Efficiency	Speed Ratio	Efficiency
0.00	0.00%	0.40	59.60%	0.80	80.53%
0.10	18.10%	0.50	69.03%	0.90	89.10%
0.20	34.06%	0.60	76.19%	0.99	98.01%

3.4 Seeding Experiments

To make successful LDV measurements, the light scattered from the probe volume must be sufficiently intense to be detected by the photomultipliers. A high quality signal will also provide ample data acquisition rates. In some cases, as in water, there are enough natural particles present to scatter sufficient light.

However, in many cases seeding particles must be introduced into the flow to increase the intensity of the scattered light. The requirements for a successful seeding particle are that it be small enough to follow the flow and large enough to generate sufficient scattered light. In addition, Menon and Lai [11] suggest that when measuring in a liquid and using a back scatter collection technique, it is desirable to have particles with a large refractive index. The seeding particles tested are listed in Table 4. Before the converter assembly was constructed, testing was conducted with the oil and particles contained in a glass jar. The jar was placed on a magnetic stirrer to create fluid motion. Only the aluminum oxide and titanium dioxide were tested initially because of the fear that the metallic coated particles might damage the internal components of the converter. The results of the early test revealed that the titanium dioxide produced the best signal and higher data rates, even though the particles are smaller. This is probably due

Table 4. Properties of seeding particles tested

Particle	Diameter	Density	Refractive Index
Aluminum Oxide (Al_2O_3)	$5.0 \mu m$	$3800 kg / m^3$	$1.76 + 0i$
Titanium Dioxide (TiO_2)	$0.2 \mu m$	$4100 kg / m^3$	$2.60 + 0i$
TSI Metallic Coated Particles	$9.0 \mu m$	$2600 kg / m^3$	$0.21 + 2.62i$

to the fact that the refractive index of the aluminum oxide is similar to that of the oil. Based on these tests, titanium dioxide was chosen as the initial seeding particle.

Initial attempts to obtain a signal in the windowed converter assembly using the titanium dioxide particles were only moderately successful. Data rates dropped off significantly as the measuring volume was moved deeper than 2 mm into the impeller passage. Although valid data was taken using this configuration, it was evident that changes needed to be made to improve the system. A TSI representative suggested trying the metallic coated particles and gave assurance that damage to the converter components would not be a problem. The oil in the system was changed and the metallic coated particles introduced. There was a noticeable improvement in signal quality. Data rates increased by an order of magnitude and signals were obtained to a depth of 20 mm inside the window.

The metallic coated particles fulfilled the light scattering requirement; however, the relatively large size caused concern about their ability to follow the flow. Two related methods were used to examine this issue. Both methods use a common parameter known as the particle relaxation time, τ , given by

$$\tau = \frac{\rho_p d_p^2}{18\mu} \quad (3.1)$$

where ρ_p is the particle density, d_p is the particle diameter, and μ is the dynamic viscosity of the fluid. The first analysis developed by Dring [12] uses the particle relaxation time in the definition of the Stokes number, St , defined as

$$St = \frac{U_c \tau}{L_c} \quad (3.2)$$

where U_c is the characteristic velocity, and L_c is the characteristic length. The analysis requires that in order for the particle to faithfully follow the flow, the

Stokes number should have a limit of $St \leq 0.01$. Using a characteristic velocity of 20 m/sec and a characteristic length of 20 mm along with particle and fluid properties from Tables 2 and 4 the Stokes number is found to be 0.006. This suggests that the particles are following the flow. The second analysis is taken from Menon and Lai [11], which examines the ability of the particle to follow rapid changes in flow velocity. Again the particle relaxation time is utilized and is used in finding the frequency response of the particle. Assuming that the particle is spherical and the density of the fluid is smaller than that of the particle, the 3 dB frequency response, f , of the particle is given by

$$f = \frac{1}{2\pi\tau} \quad (3.3)$$

Using the same values as before, the frequency response of the particle is found to be 252 KHz, which is sufficiently fast enough to follow fluctuations in the flow.

CHAPTER 4

EXPERIMENTAL PROCEDURE

4.1 Data Acquisition Checklist

The following is a checklist of the steps used to make LDV measurements in this study. Each step is expounded upon in the sections that follow.

1. The impeller and turbine rotary shaft encoder zero degree reference positions are set.
2. The measuring volume is positioned inside the Plexiglas window using the traverse table.
3. The LDV signal quality and data rate are checked.
4. The desired speed ratio is set
5. The direction and magnitude of the frequency shifts are set.
6. The data acquisition software is programmed.
7. Data is acquired. 5000 data points for each phase-one test and 10000 data points for each phase-two test were acquired.

4.2 Rotary Shaft Encoder References

The rotary shaft encoders used in the test stand allow the instantaneous positions of both the impeller and turbine to be recorded each time a velocity measurement is obtained by the LDV system. The position is measured as a function of rotation from a zero-degree reference. It is therefore important to define a known zero-degree reference for both the impeller and turbine. A

reference impeller angle of zero degrees is defined as the location where the left edge of the window is vertical at a nominal ten o'clock position. The turbine zero-angle reference is set by viewing one of the turbine blades through the window and positioning it in an easily reproducible location. The encoder puts out a 2-volt pulse each time the zero degree point is crossed, this allows the zero point to be found and set using an oscilloscope. Figure 15 shows the configuration of the window and turbine blade at their respective zero angle positions. Figure 15 is also used to define the concept and orientation of a suction and a pressure surface for a typical converter passage.

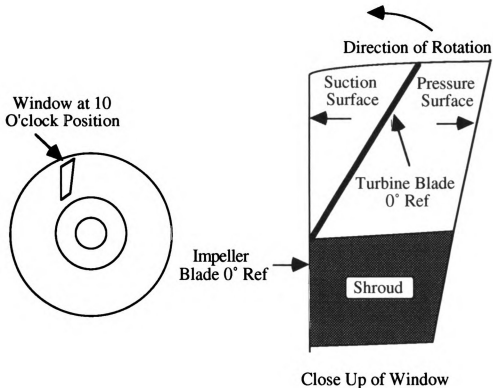


Figure 15. Position of impeller and turbine at their zero degree encoder references

4.3 Traverse Table Reference

In order to match measurement locations to discrete positions in the converter passage, the traverse table must be referenced to the torque converter assembly. The table must be referenced in all three directions. This procedure is best accomplished with the aid of the LDV laser beams. Figure 16 shows the coordinate system of the converter.

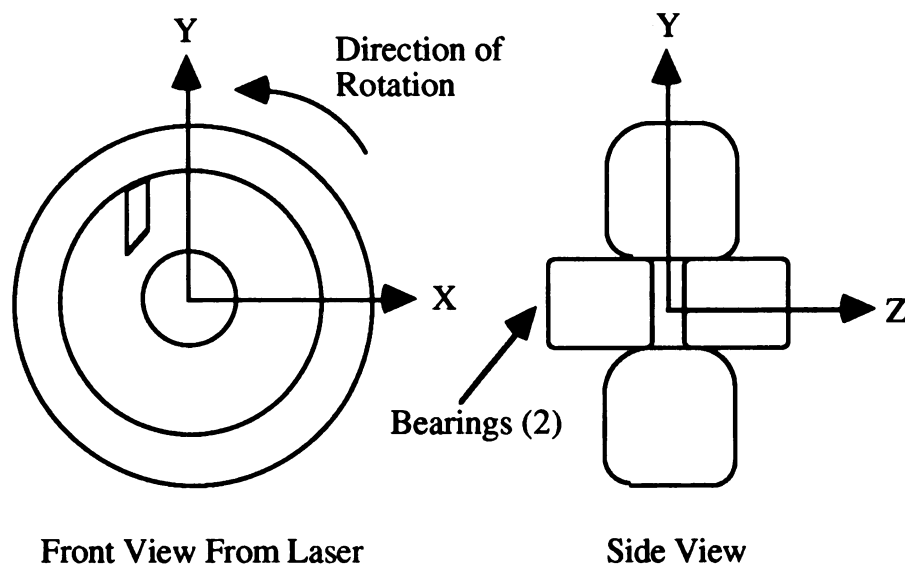


Figure 16. Traverse table coordinate system

The X and Y coordinate zero references are located at the center of rotation of the torque converter. They are set by focusing the beams at the center of the impeller side bearing, which is part of the fixture. The Z coordinate zero reference location depends on where in the impeller passage measurements were taken. For measurements in the middle of the passage, the Z zero location was defined as the interface between the window, or impeller housing, and the transmission oil. This also gave the depth of the measurement. The reference was set by viewing the

beams through the receiving optics and placing the beam crossing at the interface of the window and the fluid. For measurements near the gap region between the impeller exit and the turbine entrance, the Z zero location was defined as the XY entrance plane into the turbine passage. The reference was set by placing the beam crossing point on the tip of a turbine blade. This was accomplished by blocking one of the two beams and positioning the other beam so that it hit the tip of a turbine blade. The other beam was then unblocked and checked to ensure that it also hit the tip of the turbine blade. If it did not, the table was adjusted until both beams intersected at the tip of the turbine blade.

4.4 LDV Signal Check

The presence and quality of the scattered Doppler signal should be checked before any measurements are made. This was accomplished by placing the probe volume inside the window and driving the turbine with the dynamometer at a speed below 500 rpm. The motion of the turbine created a flow in the torque converter without causing the entire converter to rotate, thus keeping the impeller window stationary. The generation of a flow is necessary to move particles through the probe volume and produce a signal. Adjustments were made to the receiving optics so that a data rate of at least 5000 Hz was obtained. This usually ensured a nominal data rate of 100 Hz would be obtained when the converter was rotated. The signal from the photomultipliers was also checked with an oscilloscope to confirm the presence of Doppler bursts. When these criteria were met, the LDV system usually performed quite satisfactorily when the converter was operated normally.

4.5 Speed Control of the Impeller and Turbine

Speed control of the impeller and turbine was accomplished via the controllers for the 50-Hp dc drive and the 50-Hp dynamometer. Separate control of each component allowed the desired speed ratio to be established. The speed of the 50-Hp drive was set with a hand controller mounted to the test stand. The actual rpm value was calculated from the frequency of the zero point crossing signal, which is one of the output signals from the rotating machine resolver. The frequency of this signal can be measured on an oscilloscope and multiplied by 60 to find the rpm. The dynamometer controller is more versatile and can be used to set and monitor the turbine speed independently. The desired speed ratio for a particular test was set as follows. The impeller rpm was set close to the desired value using the hand controller. The speed of the turbine was set using the constant speed feature of the dynamometer controller. The controller will vary the load applied to the dynamometer to maintain the set speed. The speed of the impeller was then fine tuned with the hand controller until the desired speed ratio was attained. The speeds of both components were allowed to vary approximately 10 rpm, which results in a maximum 3 percent error in the desired speed ratio.

4.6 Frequency Shift Magnitude and Direction

Selection of the proper frequency shift and shift direction is extremely important in making valid LDV measurements. In general the direction of the shift, that is the direction that the fringe pattern will move due to the effect of the Bragg cell, should be against the mean flow. This will produce the greatest number of scattered light pulses and improve the data rate. The direction of the shift also defines what direction will be defined as being positive for the flow. The

positive direction is defined as the direction opposite to the movement of the fringe pattern. For instance, if a frequency shift of 1 MHz is used, any frequencies generated by the scattered light that are greater than 1 MHz will result in a positive velocity reading. A frequency greater than 1 MHz could only be generated in this situation if the particle is traveling against the movement of the fringe pattern, which is defined as the positive direction. Similarly, frequencies generated from scattered light that are less than 1 MHz would result in a negative velocity reading. Since the converter rotates in a counter clockwise direction and velocity measurements are made at the ten o'clock position when viewed from the laser, the frequency shift directions were chosen to make left and down as the positive directions. Data processing programs were later used to switch the coordinate system back to the more conventional standard of right and up as the positive directions. The magnitude of the shift should be great enough to measure the frequency associated with the largest negative velocity that might be encountered. The magnitude of the frequency shift used in this study varied between 2 and 10 MHz, depending on converter speed, speed ratio, and which component was being measured. In each case the value used was checked to make sure that the measured velocity range was sufficient.

4.7 Data Acquisition Software Configuration

Data acquisition was accomplished using the TSI Phase Resolved Software package (Phase) in combination with an IBM PS/2 80 computer. The software, along with some of the signal processing equipment, was specially modified by TSI to give the system the capability to track two separate rotating devices during data collection. Table 5 lists some of the experimental parameters that the software uses as inputs to provide flexibility in the data acquisition process.

Table 5. Basic TSI phase software inputs

Data File Management Information
Number of Velocity Components Measured
Amount of Data to be Collected for each Experiment
Optical Configuration of the LDV system
Rotary Shaft Encoder Configuration Information

The rotary shaft encoder configuration is especially useful in this study. The system can be configured to accept data only when the encoder values are within a specified range. Each separate rotating device can then be programmed based on the physical characteristics of the experiment, thereby ensuring that data are collected only during the time the user wishes. This ensures that no erroneous signal will be measured and collected. In this study the system software was configured to accept velocity data only when the measuring volume was within the Plexiglas window insert, which is during the first 11° of impeller rotation from its zero reference and when the turbine was at any point in its rotation. It should be noted that the software modification done by TSI requires that the two shaft encoders must be programmed individually. This was accomplished by physically moving the RS232 cable that connects the computer to the appropriate RMR, inputting the desired encoder program, and then switching the cable to the other RMR and repeating the programming step.

4.8 Data Acquisition

A specified amount of data was collected for each experiment. During the first phase of testing, 5000 data points were collected per test. In the second phase

of testing, 10000 data points were collected per test. The data points are usually evenly distributed between the two velocity components as long as the data acquisition rates are similar for both components. Typically only a few data points are collected during each rotation, or cycle, of the converter. Therefore, several thousand cycles of the converter are required to collect the specified amount of data. The velocity values are then ensemble averaged over all cycles. This assumes that the cycle-to-cycle variation in the converter flow field is negligible.

4.9 Test Envelope Development

Testing was conducted in two major phases. The initial phase concentrated on determining the feasibility of obtaining a Doppler signal from the system and what procedures produced the best results. The first attempts used titanium dioxide as the seeding material, with the receiving optics positioned in off-axis back scatter. A valid Doppler signal was obtained, but this configuration had limitations. The major limitation was the inability to measure deeper than 2 mm inside the window. Also the off-axis configuration restricted the scope of the measurement envelope. The problem was that the window mounting structure blocked the line of sight access to the probe volume, which is needed by the receiving optics to collect the scattered light. The limited line of sight access restricted the measuring envelope in two ways. First, in the side view shown in Figure 17, the line of sight access of receiving optic number 1 is restricted by the top of the window mounting structure. This limits the outer radial distance that can be measured by that receiving optic. Second, in the top view shown in Figure 17, the line of sight access of receiving optic number 2 is restricted by the side of the window mounting structure. This limits the angular coverage that can be measured by that receiving optic as the probe volume is moved deeper into the

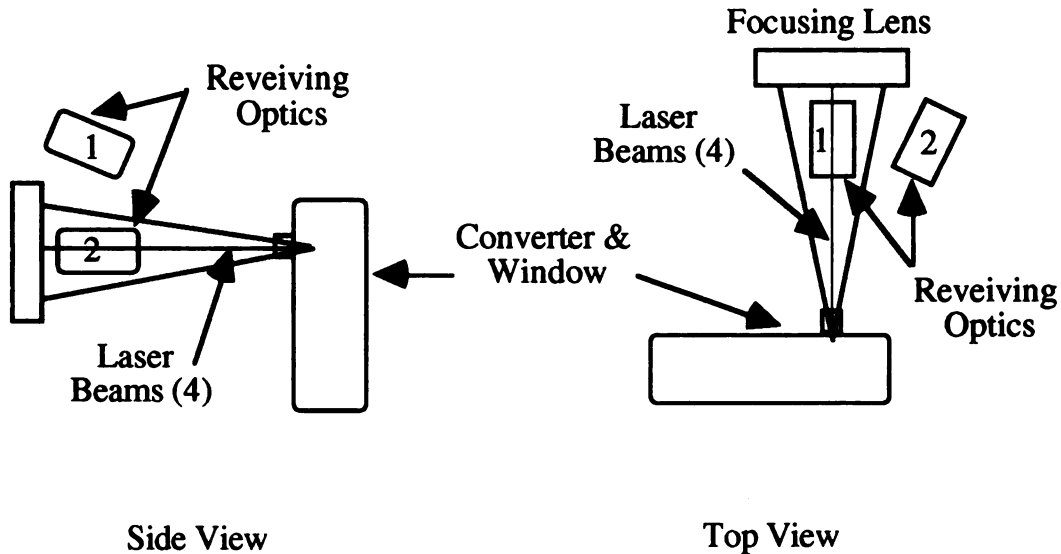


Figure 17. Off-axis back scatter configuration

window. The change to the metallic coated particles increased the scattered light intensity and alleviated the measurement depth limitation. Unfortunately the off-axis configuration still limited the angular coverage that could be measured as the probe volume was moved deeper into the passage. It became quite evident that the on-axis back scatter method would have to be employed to overcome the limitations of the off-axis configuration. The success of the on-axis back scatter technique, along with the introduction of the metallic-coated particles, vastly increased the measurement envelope. Signals could now be obtained anywhere in the passage that the laser beams could reach. This included the interface region between the impeller exit and the turbine entrance. This region provided the most interesting results and was the focus of the second phase of measurements.

Because the measuring volume remains in a fixed location and the converter window rotates past it, each experiment produces velocity information along an arc at the radius of probe volume. Usually a total of 6 out of a possible 11 degrees of angular window coverage was maintained, even as the probe volume

was moved more than 20 mm deep into the fluid.

All testing reported here was conducted at impeller speeds of either 1000 or 1500 rpm, and at speed ratios of 0.25, 0.50, 0.75, or with no-load applied to the turbine. This was based on the results of the preliminary testing that revealed the problems associated with extreme oil heating at high rpm and small speed ratios, and the deafening noise created at speeds above 3600 rpm. One successful data point was collected at a speed of 3600 rpm under a no-load condition to determine if the LDV system could make measurements at this speed, but the investigators did not wish to push the test equipment to its limits before a reasonable amount of data was collected.

CHAPTER 5

DATA PROCESSING AND DISPLAY

5.1 TSI Software Limitations

In addition to providing assistance with data acquisition, the TSI Phase software also has statistical analysis and data display capabilities. Unfortunately, these applications could not be used in this study. There are two reasons behind this. First, the statistical analysis and data display algorithms were not modified to fully integrate the data from the second rotary shaft encoder. Second, the velocity information measured by the LDV system is in an incorrect reference frame for data display. All the velocity data is referenced to an observer standing outside the converter. A more useful reference frame would be to an observer stationed inside the windowed passage, thereby making all the velocity data relative to the passage. These limitations necessitated the development of an alternative to the TSI data processing software.

5.2 Format of Initial Velocity Data

The data acquisition process produces a raw data file that contains all the pertinent information about the experiment to include the measured velocity component, its magnitude, shaft encoder values, and the cycle number when the velocity data was taken. An important assumption used in this study is that there is no cycle-to-cycle variation of the flow field. This allows a sufficient amount of data to be accumulated during the data acquisition process. The first step in processing the data is to use the TSI software to create velocity and statistical files

from the raw data. As noted in the previous section, the statistical file is not beneficial and was discarded; while the velocity information is in the wrong frame of reference and requires further processing. The velocity file was next converted from a hexadecimal format to an ASCII format with PHASEVEL, a utility program provided by TSI. A FORTRAN program was then written to convert the data to the proper reference frame and to a format appropriate for use by graphing and animation applications.

5.3 Velocity Data Conversion

A FORTRAN program was written to make data display and analysis feasible. It was designed with flexibility in mind and can be used with various converter configurations. The program prompts the user for information on the characteristics of the converter and experiment. This information includes file management data, number of impeller and turbine passages, shaft encoder specifications, impeller rpm, X and Y measurement coordinates and orientation, and the desired angular resolution describing the rotation of the impeller and turbine. The primary function of the program is to sort velocity data by the combination of impeller and turbine rotation from their respective zero references. The width of the impeller and turbine passages are divided into user-defined angular-increments. In this study, the increments used were 1° for all experiments. This meant that the windowed impeller passage had integer increments ranging from 0° to 11° , and the turbine passage values ranged from 0° to 13° . Each of the 27 turbine passages was considered to be identical. Using this logic, an impeller rotational angle of 1° and a turbine rotational angle of 2° was considered an identical configuration as an impeller rotational angle of 1° and a turbine rotational angle of 16° , 30° , 44° , and all subsequent additions of 14° , the approximate width

of a turbine passage. The values of X and Y probe volume location were used in combination with impeller rpm to calculate the converter velocity components at the measurement location. Using superposition, the program factors out the velocity contribution due to the rotation of the converter. This yields velocities that are relative to the impeller passage, the desired format. The program calculates the average velocities and standard deviations for all possible combinations of impeller and turbine rotation and writes the arrays to output files for use by graphing and animation software applications.

The problem encountered with the velocity reference frame also exists with shaft encoder information. Both encoders transmit values of rotation that are relative to an observer outside of the converter. A more useful format would be to know the position of the turbine blades relative to an observer sitting in the impeller passage. This is especially important when the data is to be used in an animation application. Figure 18 helps illustrate this point.

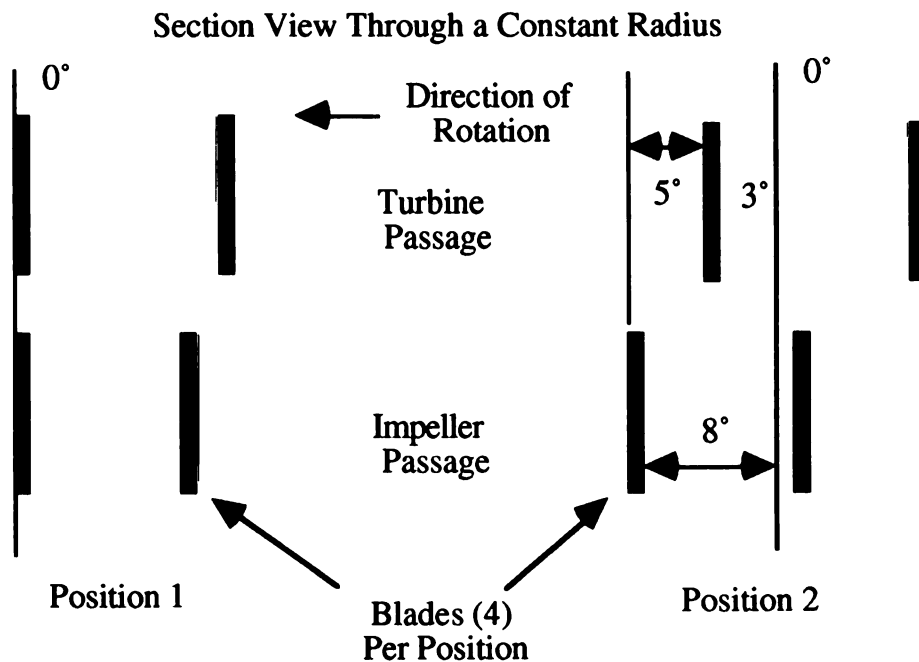


Figure 18. Illustration of relative impeller and turbine blade position after rotation

A section view of simplified impeller and turbine blades is shown in Figure 18. Position 1 shows the alignment of impeller and turbine blades and their respective passages at the zero-degree reference positions. Position 2 shows their alignment after some arbitrary rotation. In Position 2 the impeller shaft encoder would transmit a value of 8° of rotation and the turbine encoder would transmit a value of 3° . These are the values that an observer outside of the converter would also see; however, an observer sitting in the impeller passage would say that the turbine blades are offset 5° relative to where they started. This is the value that is used in the animation program that uses the observer sitting in the impeller passage as the reference frame. Consequently, an additional array with the proper impeller and turbine rotational relationship was written to the output file for use with the animation program.

Plots of velocity and standard deviation versus impeller and turbine angle were produced using Microsoft Excel. Because the flow field in the converter is very complicated, these simple plots were insufficient in attempts to visualize the relationship between the flow and the various components of the converter, especially near the interface region between the impeller and the turbine. For this reason PV~WAVE, an animation software application from Precision Visuals, was employed to gain a better understanding of the flow phenomena near this region.

CHAPTER 6

RESULTS AND DISCUSSION

6.1 Phase One Results

The limitations of the off-axis back scatter technique and titanium dioxide seeding particles severely restricted the measurement envelope of the first phase of measurements. Table 6 summarizes the test envelope.

Table 6. Measurement envelope for the first phase of testing

Radial Position (mm)	Depth In Window	Impeller Rpm	Speed Ratios Measured			
			No Load	0.75	0.5	0.25
93.5	2 mm	1500	√	√	√	
94.3	2 mm	1000	√		√	√
94.3	2 mm	1500	√		√	√
96.9	2 mm	1000	√	√	√	√
96.9	2 mm	1500	√	√	√	√
98.7	2 mm	1500	√	√	√	√
104.9	2 mm	1000	√		√	√
104.9	2 mm	1500	√		√	√

X and Y velocity component measurements at a radius of 94.3 mm, 2 mm depth, 1000 rpm, and three different speed ratios are shown in Figures 19 through 24. These plots are typical of phase one measurements. The plots show velocity versus a combination of turbine and impeller angle. The no-load speed ratio refers to the test condition when no resistive load was applied to the turbine. The only load incurred by the turbine was due to friction in the fixture bearings. It is as

close to a one-to-one speed ratio as could be simulated with the test stand.

The first item examined was the relationship between velocity and the instantaneous position of turbine blades. Since the turbine rotates at a slower speed than the impeller, the blades in effect continually pass in front of the impeller exit plane. The physical nature of the device would suggest that the blade passing would have a noticeable effect on the flow. However, an examination of Figures 19 through 24 does not support this. In all cases there is no evidence of velocity dependence on the instantaneous position of the turbine. This finding is similar to that of Bahr [7].

There are several trends that emerge upon examination of Figures 19 through 24. The first can be seen by comparing the velocities at the no-load speed ratio to those at the 0.50 speed ratio condition. Under the no-load condition, the velocity magnitudes are relatively small and uniform for all impeller angles. This is expected since under no-load conditions, both the impeller and turbine spin at nearly the same speed and the centrifugal force they impart to the fluid is approximately equal. As a result, there is little net flow through the fluid circuit. As the turbine speed slows, the centrifugal force it generates decreases and there is less resistance to flow through the fluid circuit. The net result is an increase in the flow through the circuit [1]. An increase in circuit flow for measurements taken during phase one would be most evident in the Y velocity component, since the orientation of the impeller passage is nominally vertical during data acquisition. In the no-load case shown in Figure 19, the Y velocities are on the order of 0.5 m/s. In the 0.50 speed ratio case shown in Figure 20, they increase to 5.0 m/s. There is a definite increase in the flow through the fluid circuit from no-load to a 0.5 speed ratio, as is expected. In Figures 22 and 23, the magnitude of the X velocities does not change significantly as the speed ratio changes to 0.50, but the values become more diverse and a velocity dependence on the impeller angle

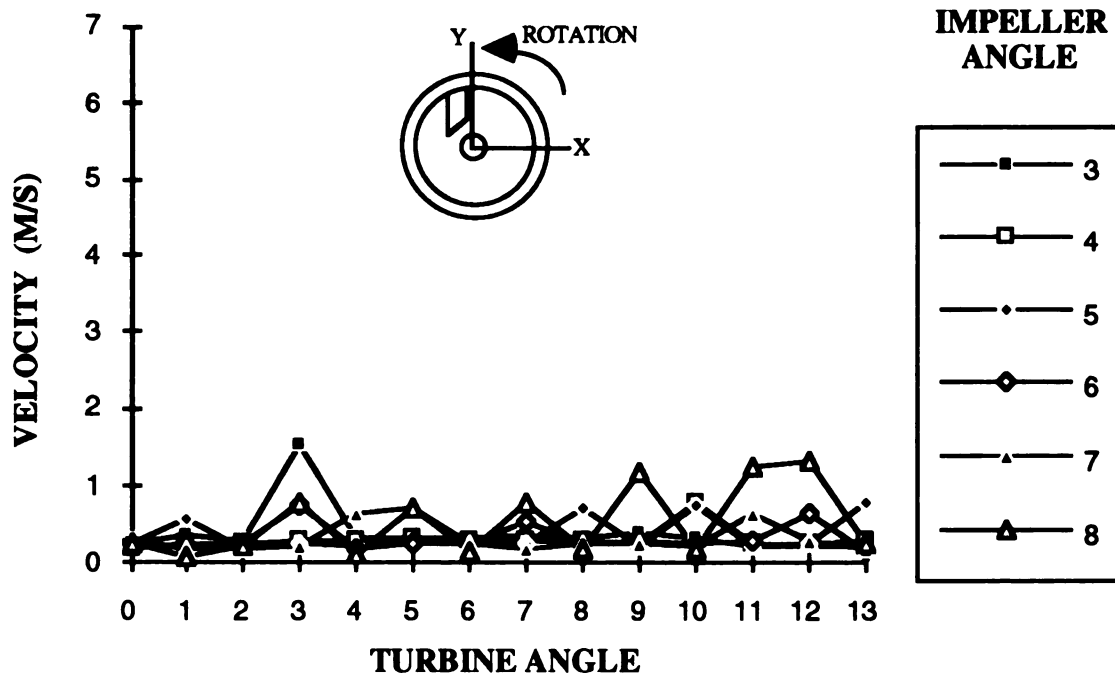


Figure 19. Y velocity components at 1000 rpm and no-load speed ratio

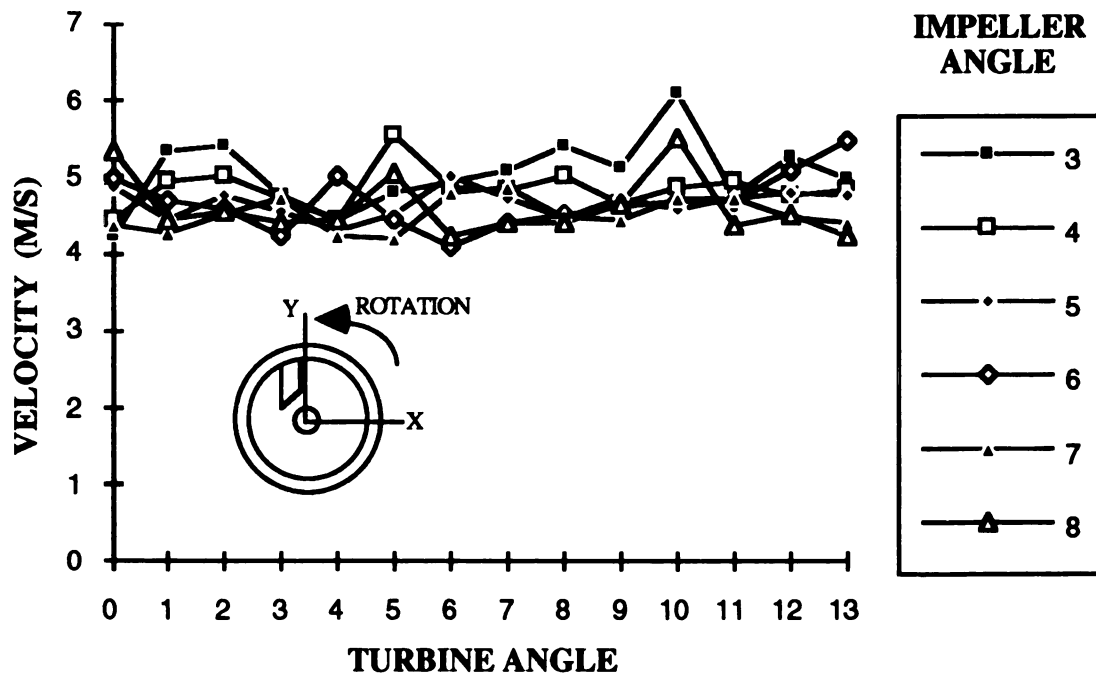


Figure 20. Y velocity components at 1000 rpm and 0.50 speed ratio

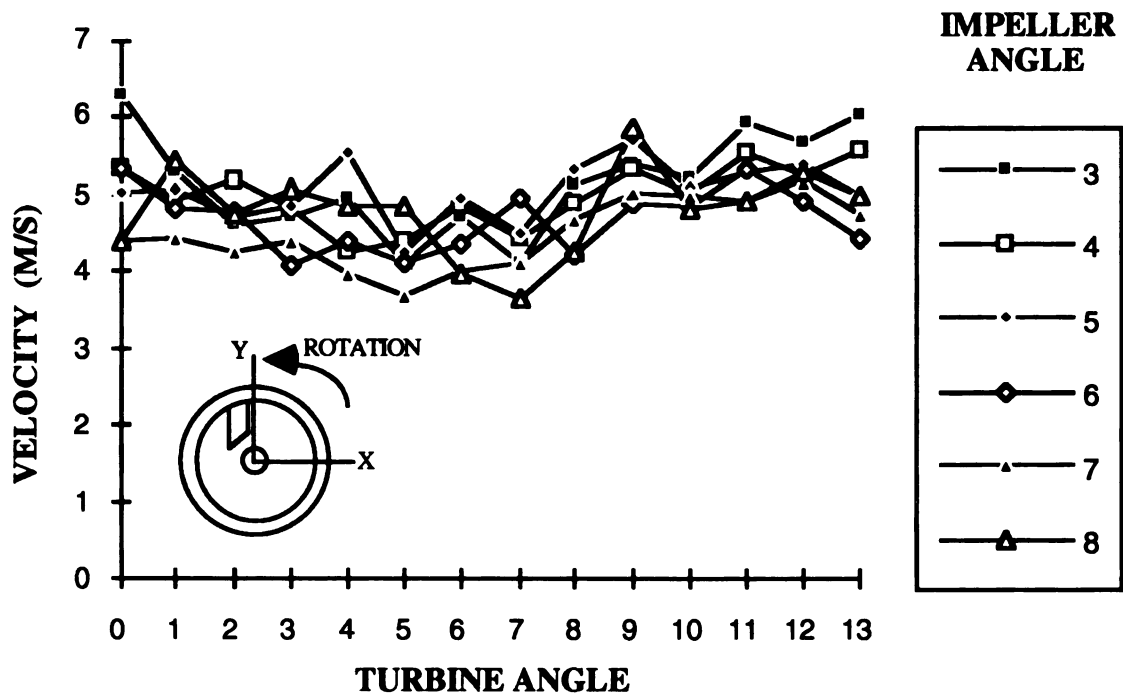


Figure 21. Y velocity components at 1000 rpm and 0.25 speed ratio

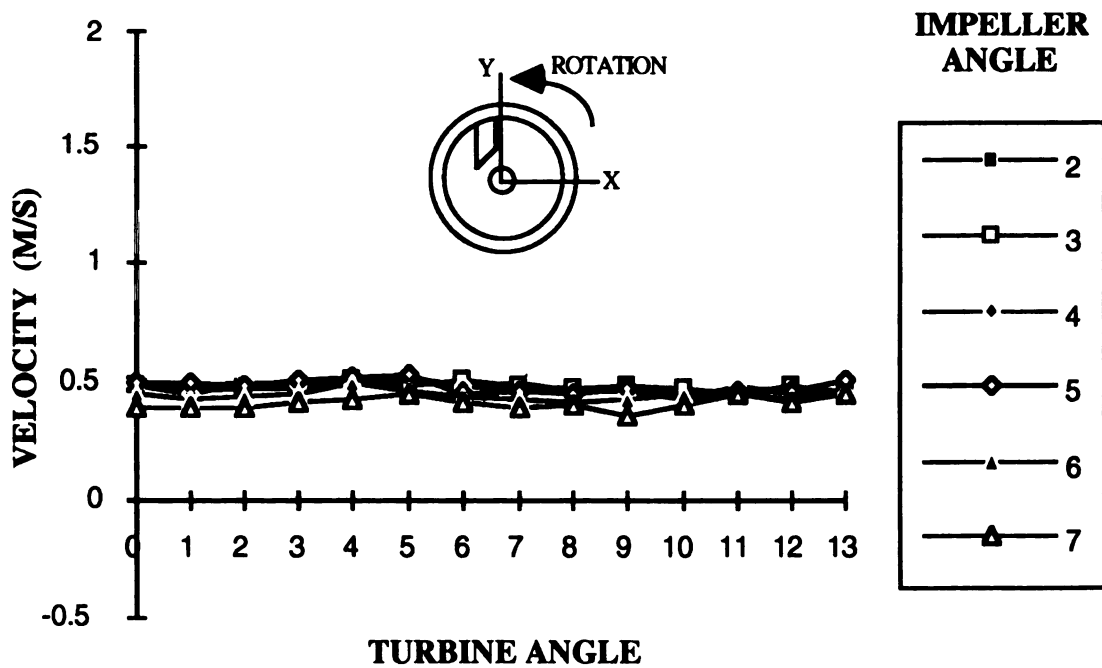


Figure 22. X velocity components at 1000 rpm and no-load speed ratio

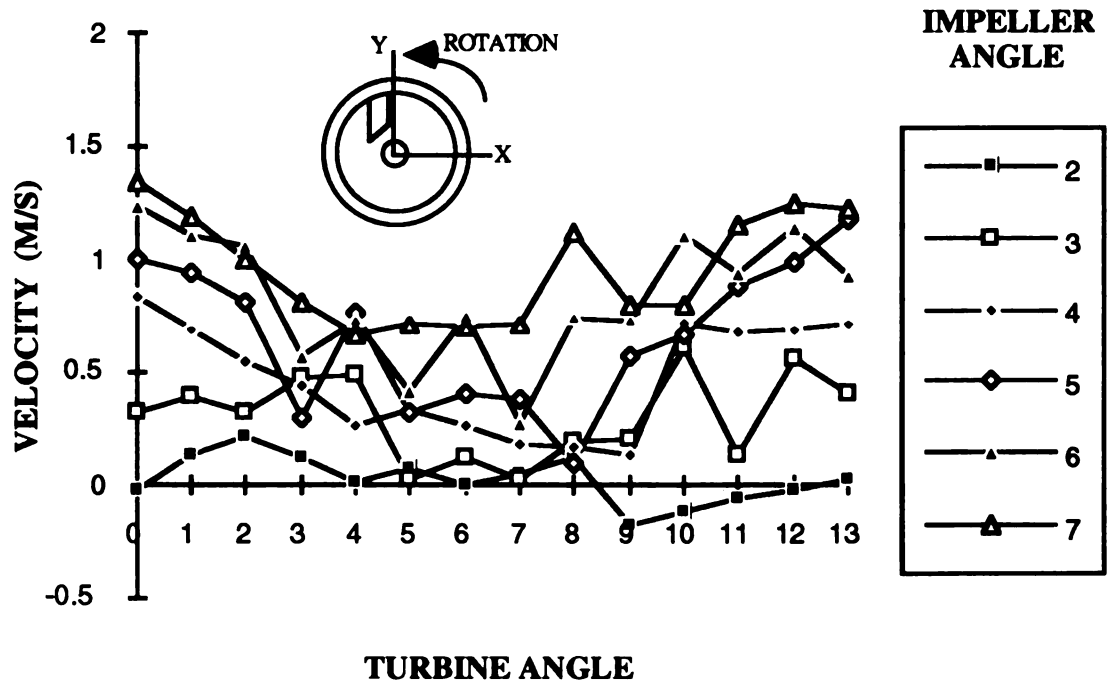


Figure 23. X velocity components at 1000 rpm and 0.50 speed ratio

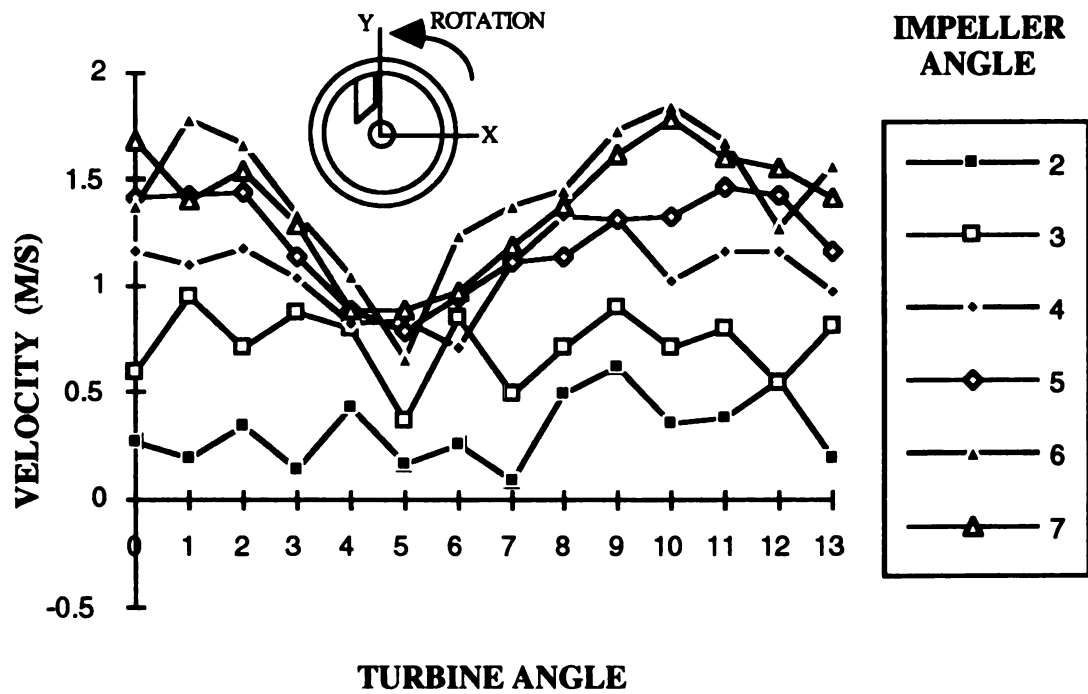


Figure 24. X velocity components at 1000 rpm and 0.25 speed ratio

is evident. The magnitude of the velocities are smaller at locations nearer to the suction surface and larger near the pressure surface. This is consistent with the findings of Numazawa [8].

Since there was such a substantial increase in circuit flow when the speed ratio was reduced by a factor of 2, one might expect a similar increase with a further reduction of the speed ratio. A comparison of the plots for the 0.50 and 0.25 speed ratio cases does not support this. The magnitude of the Y velocities from Figures 20 to Figure 21 only increase slightly, and the dependence on impeller angle remains unchanged. The magnitude of the X velocities from Figures 23 to Figure 24 remain similar, and the variation due to impeller angle becomes more defined. There is not the same increase in circuit flow as from the no-load to the 0.50 speed ratio case. Evidently, further reducing the speed ratio has an effect on the flow other than to increase the flow rate. An examination of the standard deviations of the velocity measurements may reveal this other characteristic. The standard deviation of velocity measurements can also be thought of as a measure of flow turbulence, the larger the standard deviation, the more turbulent the flow [13]. Figures 25 and 26 show the standard deviation of the velocity measurements plotted against the impeller angle only, since no dependence on turbine angle is evident. The plots show that as the speed ratio is reduced, the standard deviations of the velocities increase and the flow is more turbulent. Apparently there is a maximum flow rate that can be achieved by reducing the speed ratio and, therefore, the resistance to the flow. Any further reduction in speed ratio acts mainly to increase the turbulence of the flow.

Data taken at the other locations for the first phase of measurements showed similar trends to those described above.

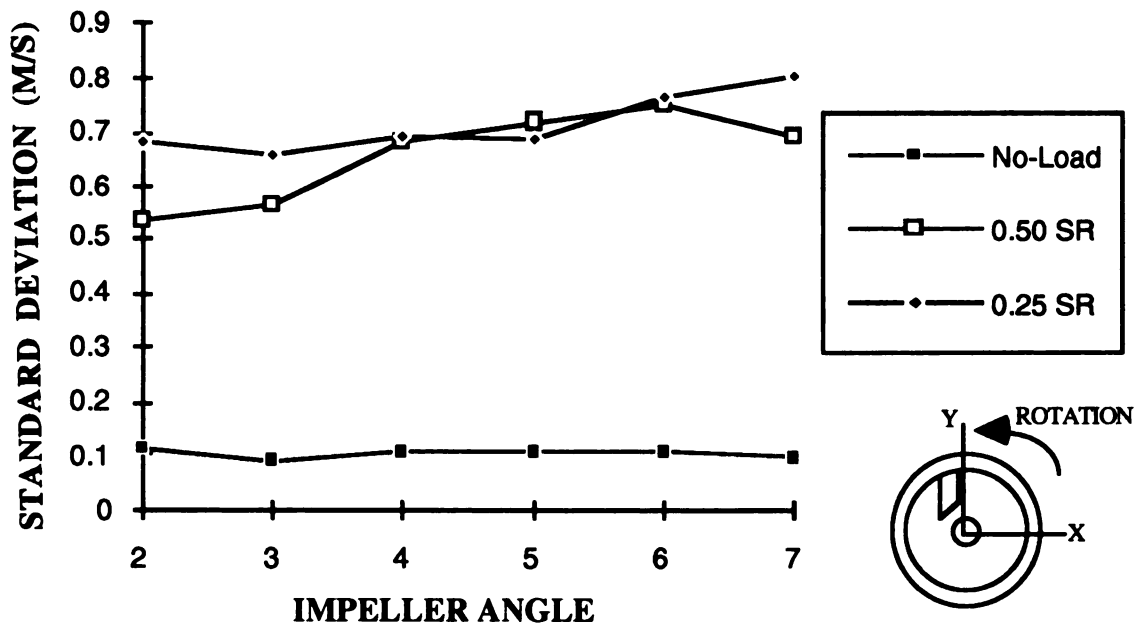


Figure 25. Standard deviations of X velocities independent of turbine angle

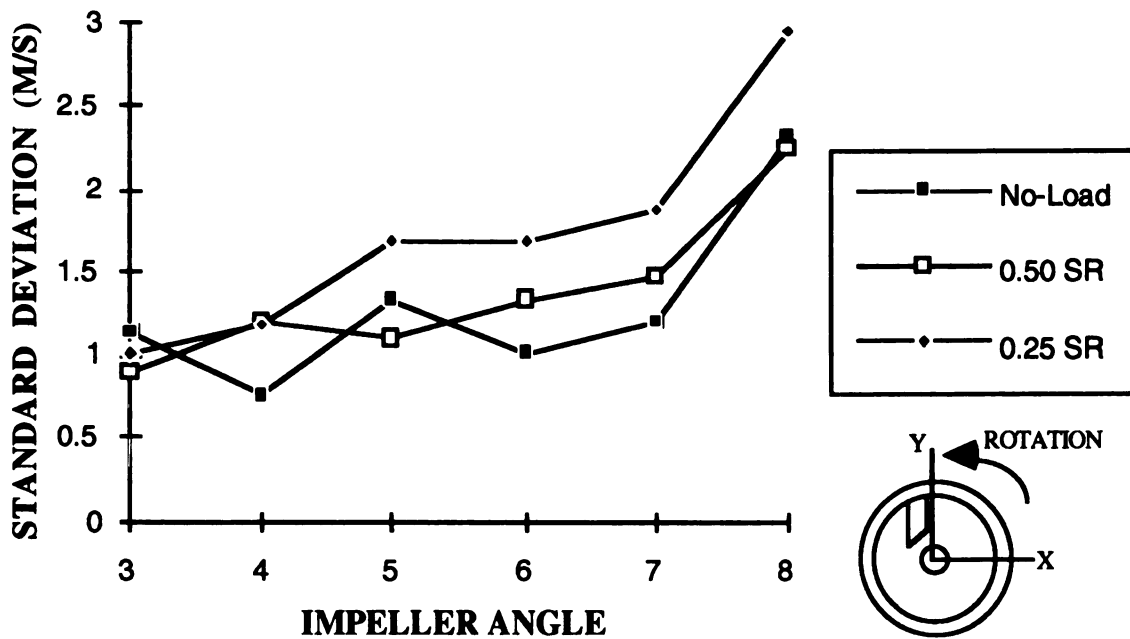


Figure 26. Standard deviations of Y velocities independent of turbine angle

6.2 Phase Two Results

The combination of the on-axis back scatter technique and use of metallic-coated seeding particles significantly improved the measurement envelope of the data taken in this study. The region containing the impeller exit and turbine entrance planes was able to be measured. This region is of particular interest since the characteristics of the flow are largely unknown and therefore difficult to model. Of particular interest was to again examining the effect, if any, that the turbine blade passing has on the flow exiting the impeller. In phase one this effect was not present. Table 7 summarizes the test envelope for the second phase of measurements.

Table 7. Measurement envelope for the second phase of testing

Radius (mm)	Range of Z Positions From Turbine (mm)	Impeller Rpm	Speed Ratios Measured		
			0.75	0.5	0.25
107	-5:-4:-3:-2:-1:0:1:2	1000	√	√	√
110	-5:-4:-3:-2:-1:0:1:2	1000	√	√	√
113	-5:-4:-3:-2:-1:0:1:2	1000	√	√	√
107	-5:-4:-3:-2:-1:0:1:2	1500	√	√	√
110	-5:-4:-3:-2:-1:0:1:2	1500	√	√	√

Figures 27 through 29 show the X velocity components for measurements taken at a radius of 110 mm, 1000 rpm, 0.50 speed ratio and for Z coordinates of -2, -1, and 0 mm before the entrance plane to the turbine passage. The velocity profile shown in Figure 27 is very similar to those found during the first phase of testing. There is no noticeable dependence on turbine angle, and the velocity near

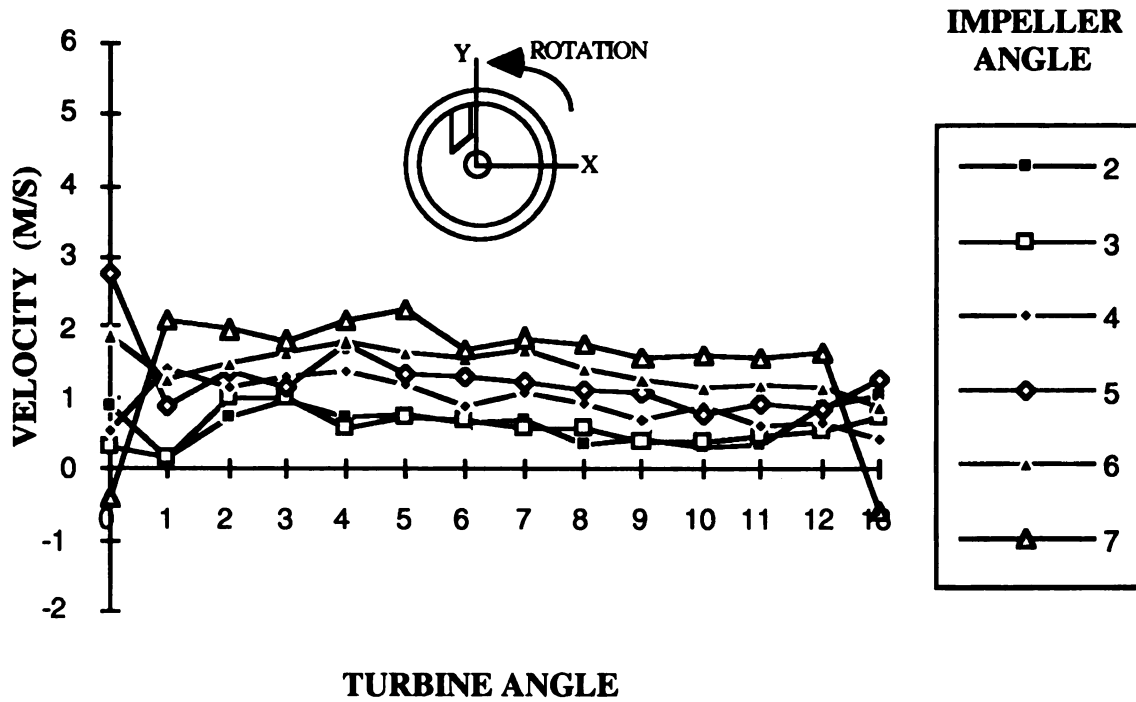


Figure 27. X velocity components 2 mm from turbine entrance, 0.50 speed ratio

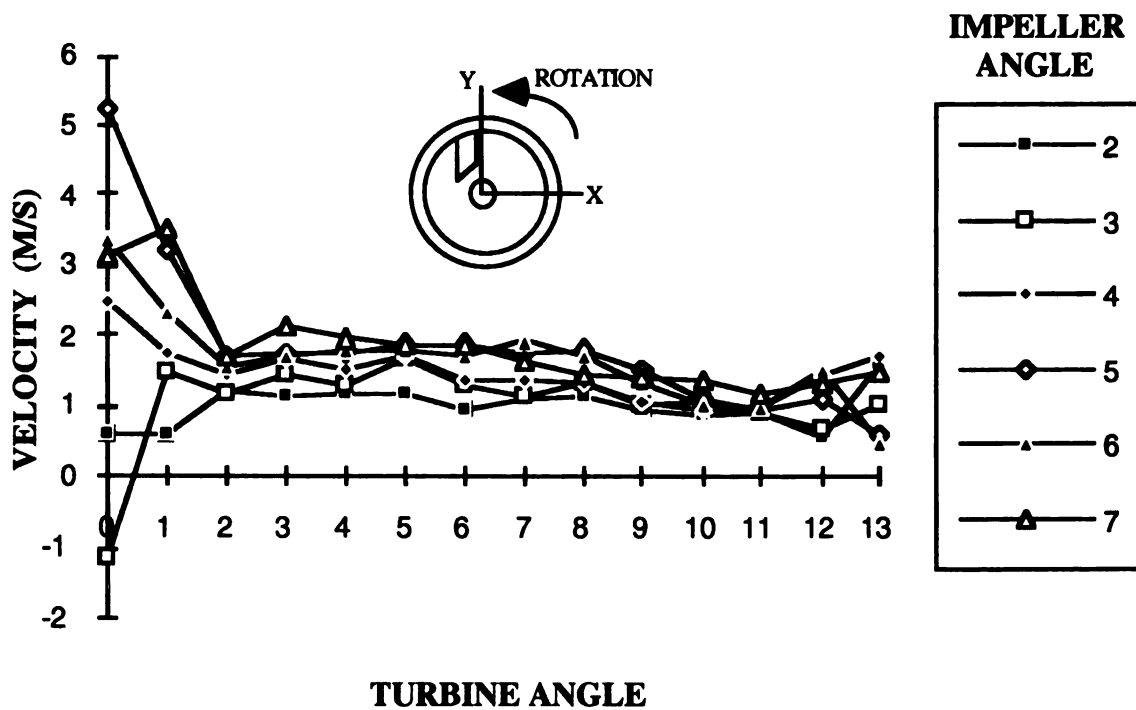


Figure 28. X velocity components 1 mm from turbine entrance, 0.50 speed ratio

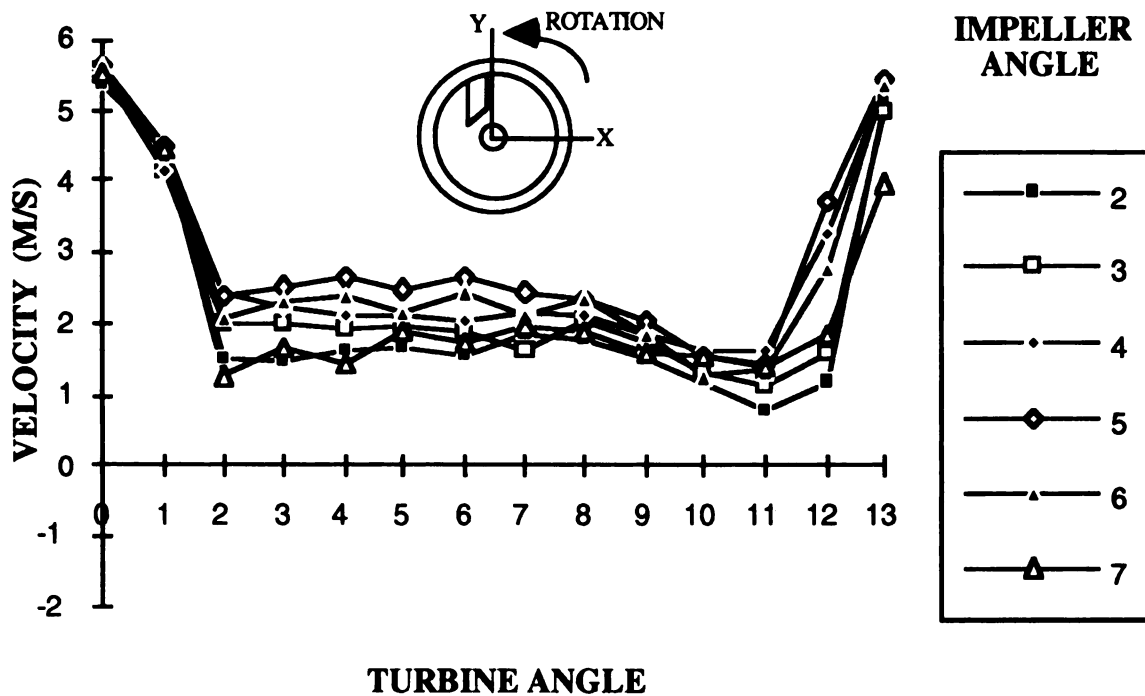


Figure 29. X velocity components at the turbine entrance plane, 0.50 speed ratio

the pressure surface is larger than near the suction surface. However, as the measuring volume is moved closer to the entrance plane, the similarity ends. In Figure 28, a dependence on turbine angle can be seen at turbine angles between 0° and 2°. In Figure 29, the velocity profile has developed a definite dependence on the turbine angle. At turbine angles between 11° and 2°, which is actually a continuous segment of a rotation, the velocity increased in magnitude from 2 m/s to over 4 m/s. For the first time the effect of the instantaneous position of the turbine blades can be seen. Figures 30 through 32 show the Y velocity components for the same positions. As was the case with the X components, there is not a noticeable dependence on the instantaneous position of the turbine until the flow reaches the plane 1 mm prior to the turbine entrance.

The small magnitude of the Y velocity components shown in Figures 30 through 32 is due to the fact that the physical orientation of the impeller passage at

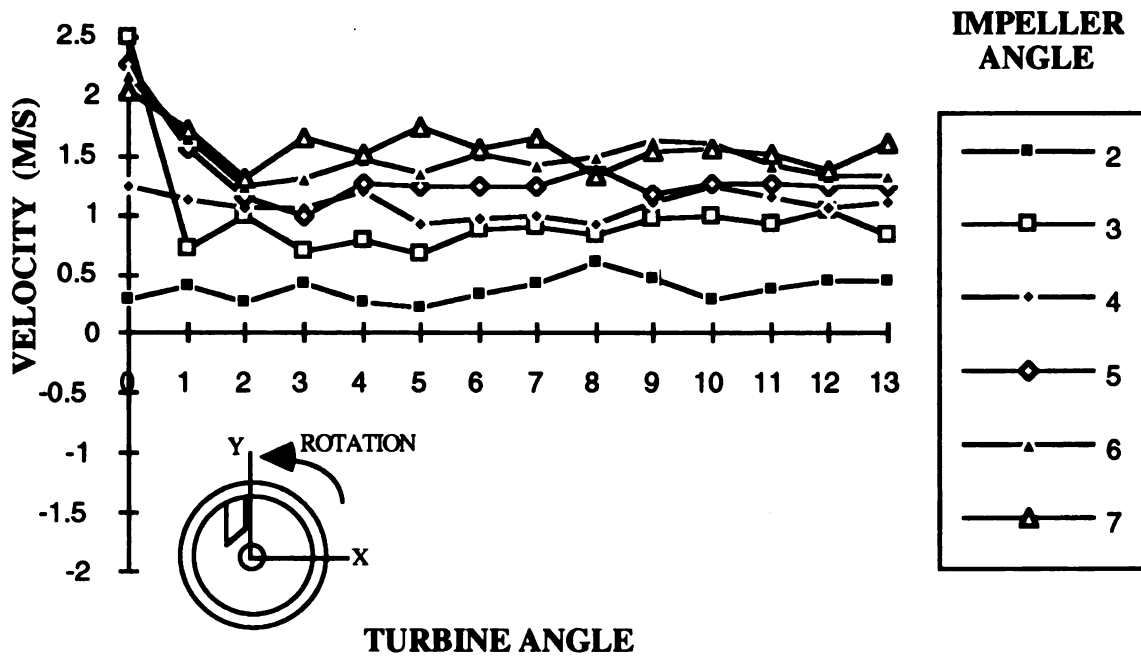


Figure 30. Y velocity components 2 mm from turbine entrance, 0.50 speed ratio

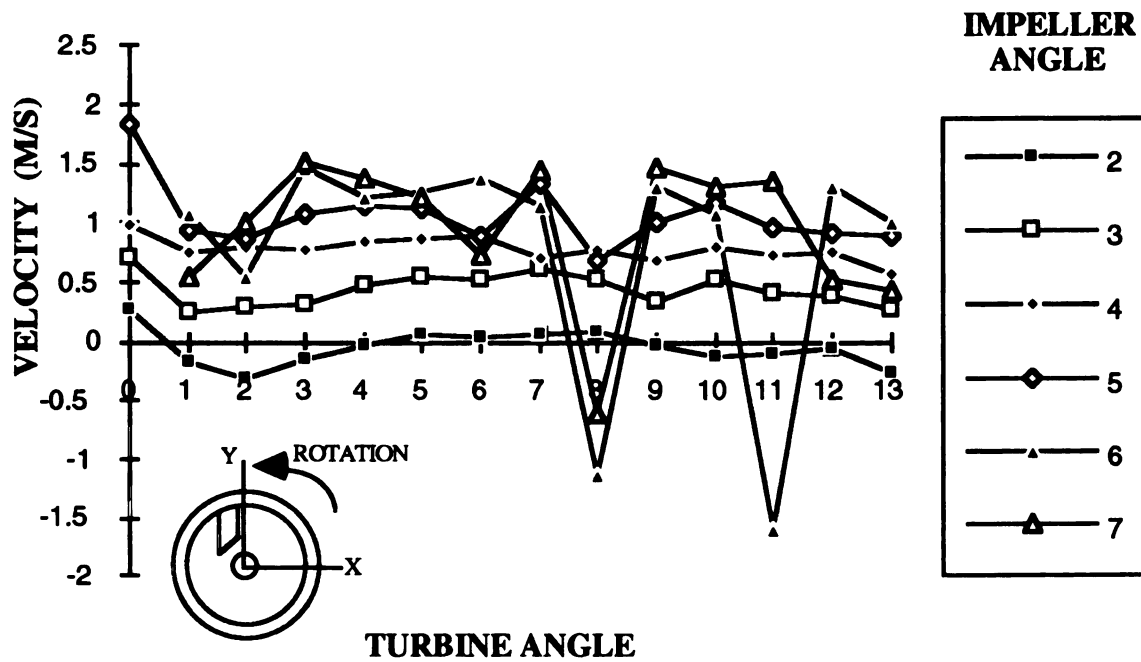


Figure 31. Y velocity components 1 mm from turbine entrance, 0.50 speed ratio

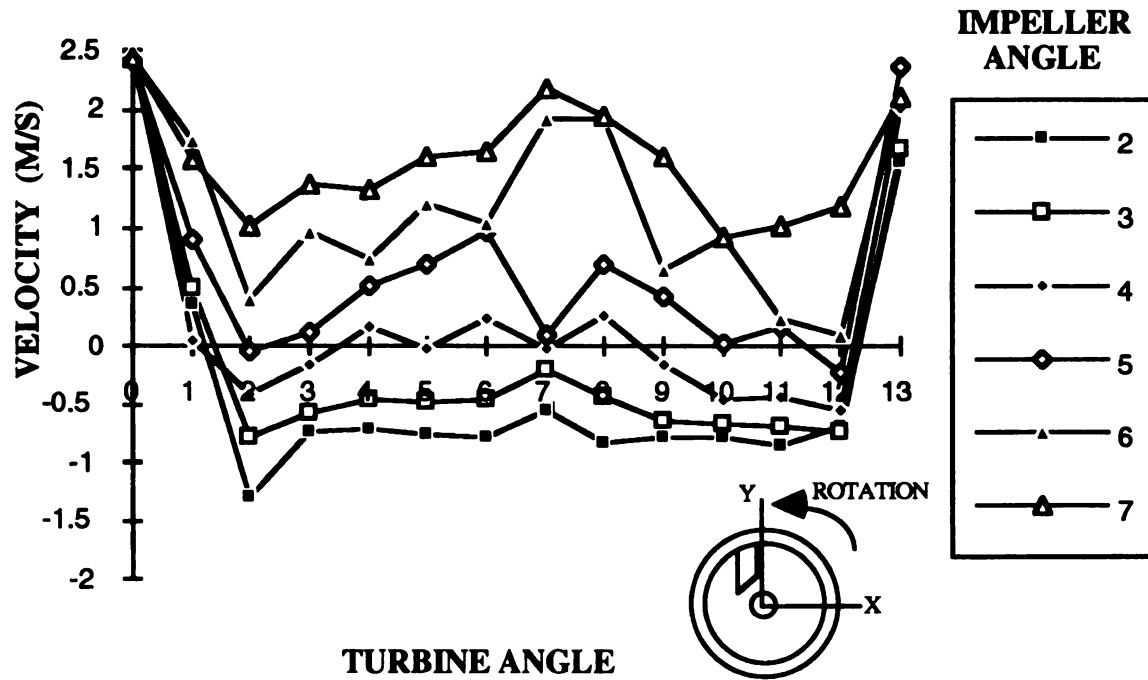


Figure 32. Y velocity components at the turbine entrance plane, 0.50 speed ratio

probe volume locations for the second phase of measurements was nominally horizontal. In this area of the passage the X and Z components are the most important in describing the flow. The LDV system cannot measure the Z component as it is currently configured. A closer examination of the X components may reveal some interesting insights into the flow. In Figures 33 and 34 the 0.75 and 0.25 speed ratio cases of X velocities are plotted for the same conditions described in Figure 29. As the speed ratio is reduced, the velocity of the flow increases and the dependence on turbine angle becomes more evident. The velocity is also greater near the pressure surface. Except for the dependence on turbine angle, these are all similar traits exhibited by the data from phase one.

The standard deviations of the X velocity components are shown in Figures 35 through 37. In all three cases the standard deviations are relatively small and constant for turbine angles between 2° and 11°. This is same range of turbine

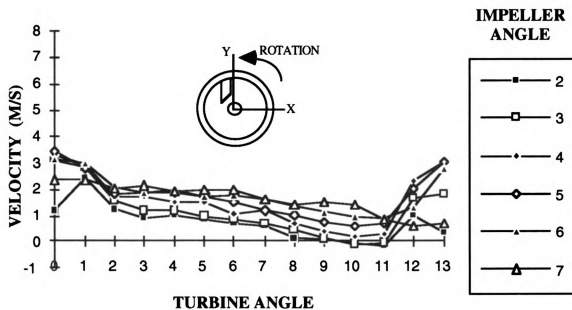


Figure 33. X velocity components at the turbine entrance, 0.75 speed ratio

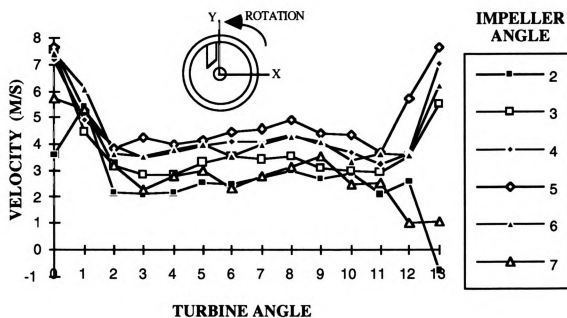


Figure 34. X velocity components at the turbine entrance plane, 0.25 speed ratio

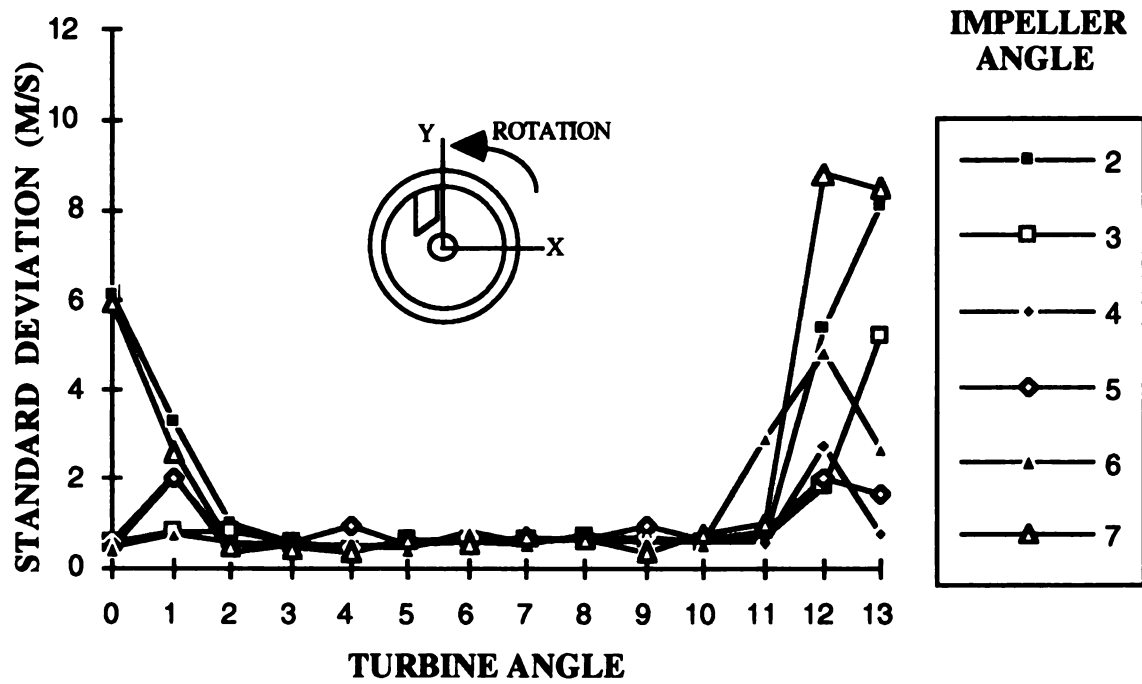


Figure 35. X velocity standard deviations at turbine entrance, 0.75 speed ratio

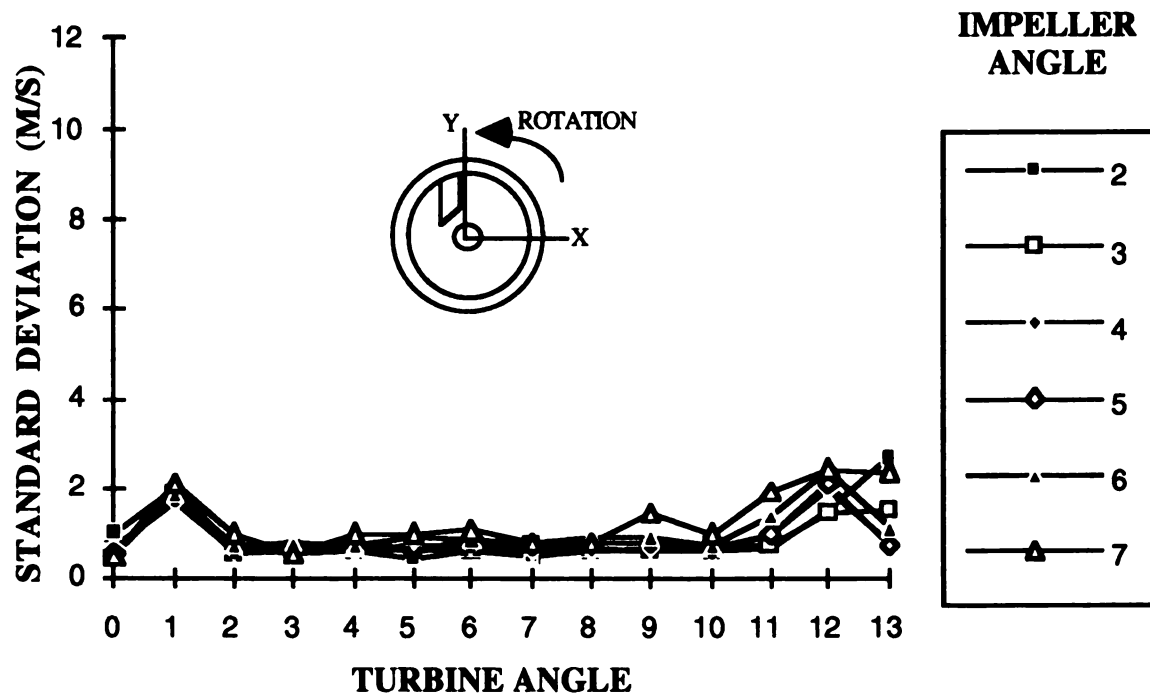


Figure 36. X velocity standard deviations at turbine entrance, 0.50 speed ratio

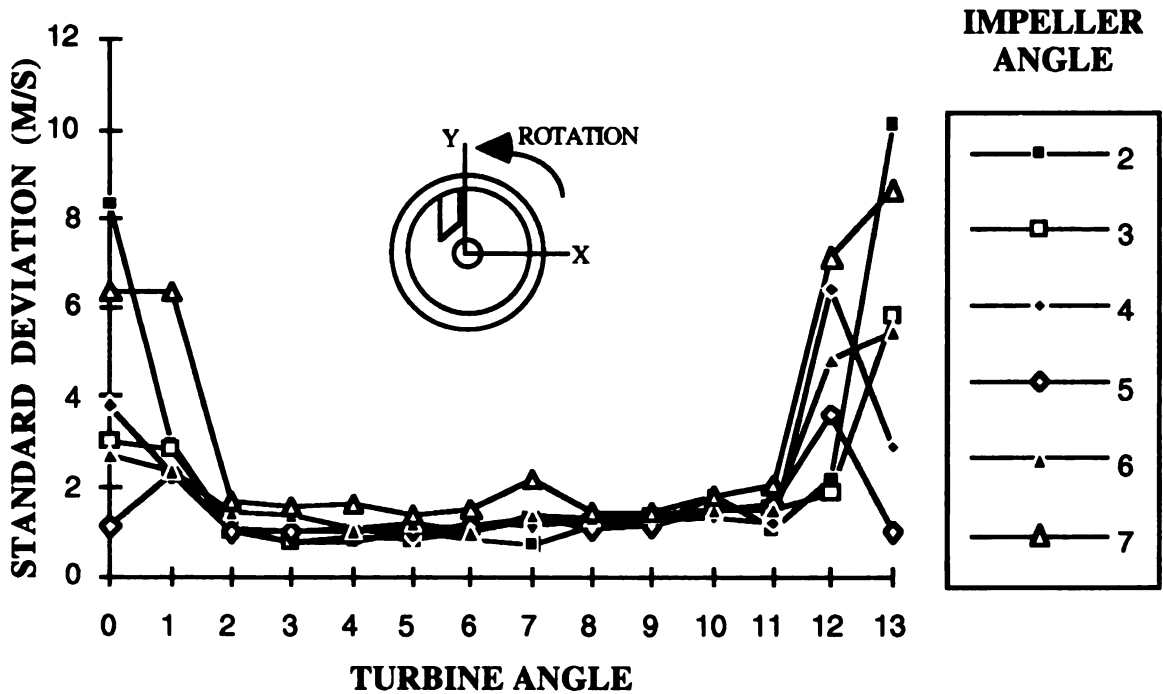


Figure 37. X velocity standard deviations at turbine entrance, 0.25 speed ratio

angles where the velocity values are constant. In the range between 11° and 2° the standard deviations vary greatly. This region of the flow is extremely turbulent.

One of the flow characteristics of interest is the entrance angle of the flow into the turbine. This angle would be found from the X and Z velocity components. Many current models assume the inlet flow into the turbine is steady and uniform. Although information on the Z component is not available, the information obtained on the X components would seem to dispute the assumption of steady and uniform flow.

A better understanding of the flow phenomena at the interface region is needed to aid in the modeling process. Trying to visualize the flow in the converter is extremely difficult. The absence of the third velocity component data compounded the problem. The plots of the velocity data used to this point do not provide the broad scope of information necessary to reveal important flow

characteristics. This drove the decision to use PV~WAVE to animate the flow velocity vectors in hopes of gaining a better overall understanding of the flow in the gap region.

The frames for the movies were produced on a Sun work station at the MSUERL using PV~WAVE. The frames were then animated at the Case Center and placed on a VCR format. It must be pointed out that because information on the third velocity component is not available, only educated guesses and not conclusions can be drawn from these movies.

Three different sets of animated movies were made. In the first set of animations, a top view of the X velocity components are plotted for a given radius, impeller speed, and speed ratio. Data from each of the eight Z positions were included. Figure 38 shows the animation of the velocity measurements taken at a speed of 1000 rpm, 110 mm radius, and a 0.50 speed ratio. The frames show the velocity field at each of the 14 incremental locations of the turbine blade. For simplicity, the turbine blades are represented with a small leading edge segment of a single blade. Dotted lines are used to show the outline of the pump passage. Examination of Figure 38 reveals several interesting trends. One is that as the turbine blade travels past the impeller exit, the fluid immediately in front of it is accelerated. This can be seen for turbine blade positions between 1° and 8° , the period when the turbine blade is in the region that the LDV system can measure. As the turbine blade moves out of the measurement region, from 9° to 0° , the flow tends to settle down and become steady. Probably the most important trend shown by Figure 38 is evidence of a secondary flow. This evidence is contained in the frames for turbine positions of 1° through 8° . A close examination shows that the velocity of the fluid in the gap region where the turbine has just passed is either significantly reduced or reversed. For instance, when the turbine blade position is 3° , the flow velocity at a pump window angle of 3° and a Z position of -1 mm has

reversed. This suggests that the leading edge of the turbine blade may generate a vortex that could be a source of secondary flow. This secondary flow would cause a reduction in the efficiency of the converter. This phenomena should appear in a numerical simulation of this region. Only the flow in the gap region seems to be affected. The flow 3 mm to 5 mm from the turbine entrance, which is inside the impeller passage, is relatively unaffected. This is consistent with the plots of the X velocity vectors shown in Figures 27 through 29, where the instantaneous position of the turbine blade did not have a noticeable effect of the flow until the flow entered the gap region. Animations for flow at other radii and conditions revealed similar findings. Obviously the flow in the gap region is very complicated and magnifies the need to obtain information on the third velocity component. Knowledge of the Z velocity component would allow the instantaneous flow entrance angle to be found as well as quantifying any secondary flow.

In the second set of animations, a front view of the resultant vectors were constructed from the individual X and Y velocity components and plotted for a given impeller speed and speed ratio at each of the eight Z position planes. Each plot contains the velocity vectors at the given radius and angular rotational position of the window. The dotted lines represent the impeller blades and the leading edge of a turbine blade is displayed. Figure 39 shows the animation of the velocity measurements taken at 1000 rpm, 0.50 speed ratio, and at the entrance plane to the turbine. Again the frames show the velocity field at each of the 14 incremental locations of the turbine blade. Patterns similar to the animation of the X velocity components in Figure 38 are present in Figure 39. For instance, at turbine positions between 1° and 5° the flow near the turbine blade is accelerated at each of the three radii. The flow behind the turbine blade has decreased in magnitude which would support the theory surmised from the first animation that

the turbine blade generates a vortex and subsequently a secondary flow. As the turbine blade moves out of the measurement region, turbine blade positions 6° through 1° , the flow becomes more steady. The second animation did reveal another interesting aspect of the flow near the gap region. There is evidence that some fluid located behind the impeller shroud is reentering the main flow. In Figure 39 at turbine positions of 4° and 5° and at a radius of 107 mm there is a velocity vector in the outward radial direction that would suggest that fluid from behind the shroud is reentering the flow. Similar velocity vectors are present in animations of other planes near the turbine entrance. Again, such a leakage flow should be modeled in a numerical simulation.

The third set of animations are a three-dimensional overview of all eight planes from the second set of animations. These animations provide a better perspective on the presence of secondary flows and also confirm that fluid appears to be reentering the main flow from behind the shroud.

The animations have proved to be valuable tools in helping to understand some of the flow phenomena in the impeller exit and turbine entrance region. However, only when information on the third velocity component is obtained can definite conclusions on the flow be made.

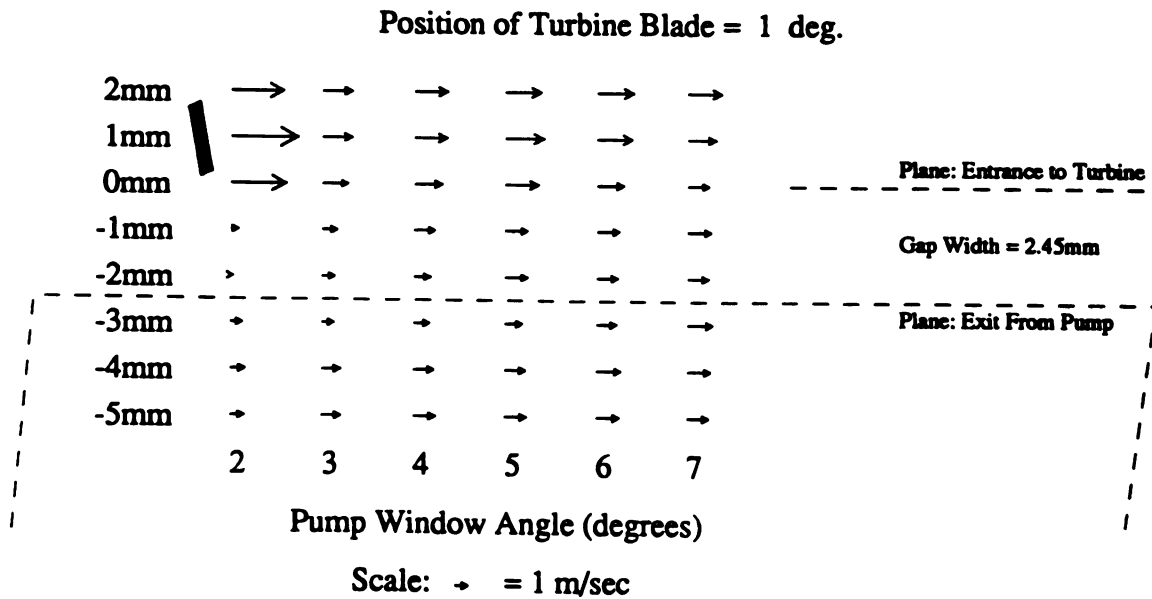
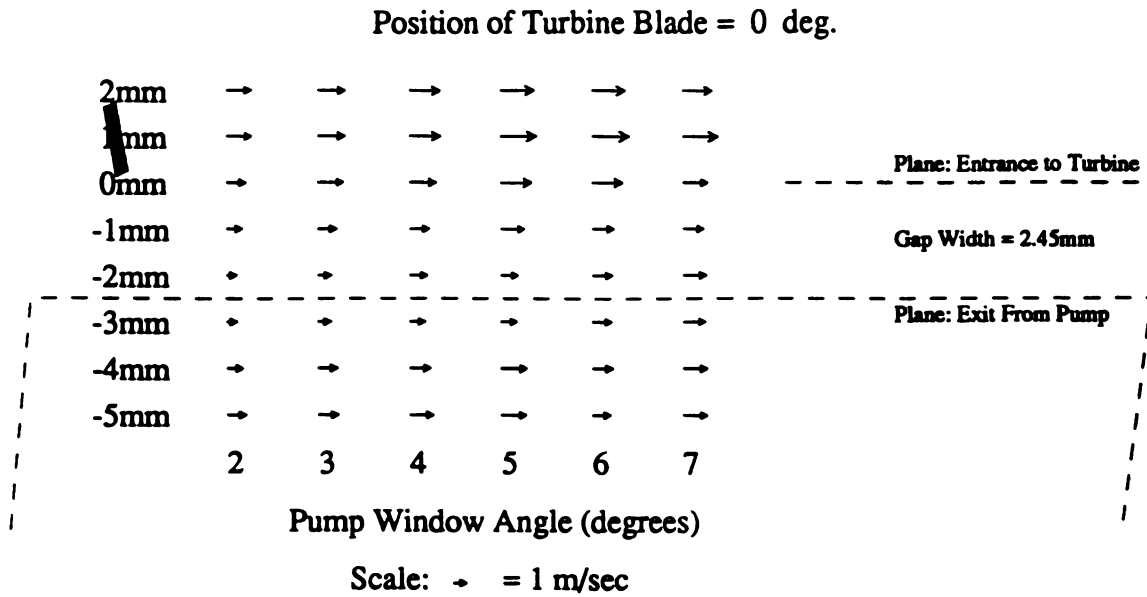


Figure 38. X velocity vectors at 1000 rpm, 110 mm radius, and a 0.50 speed ratio

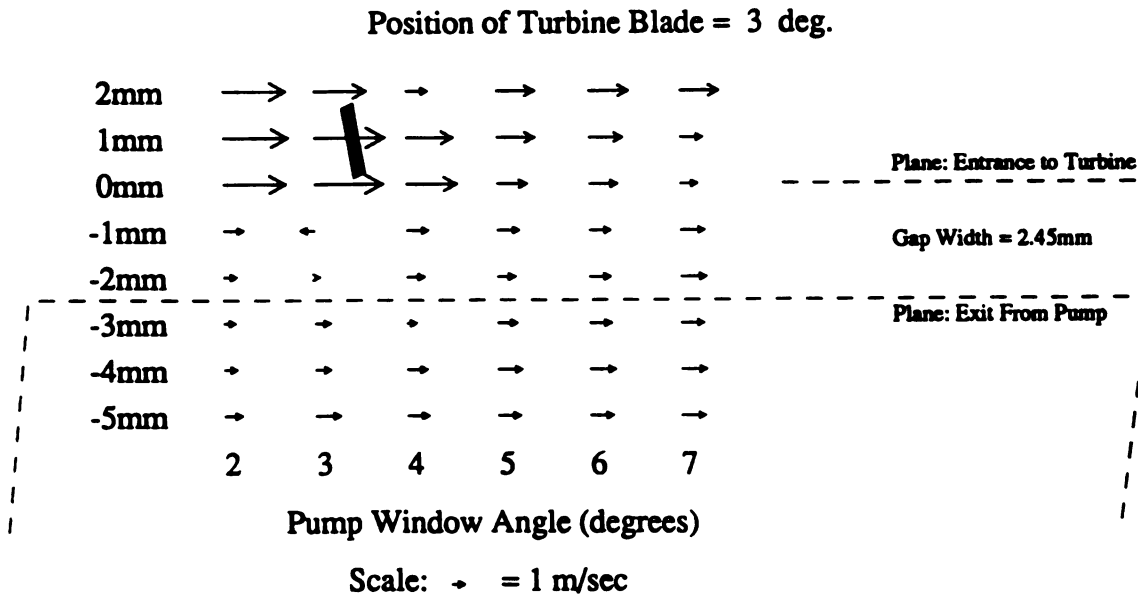
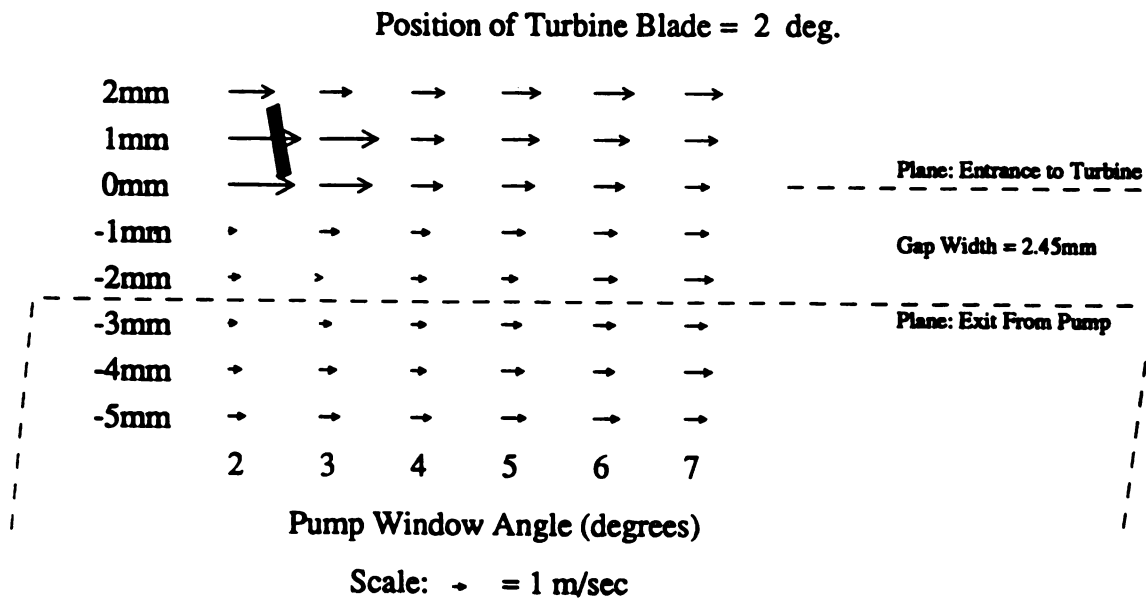


Figure 38. (continued)

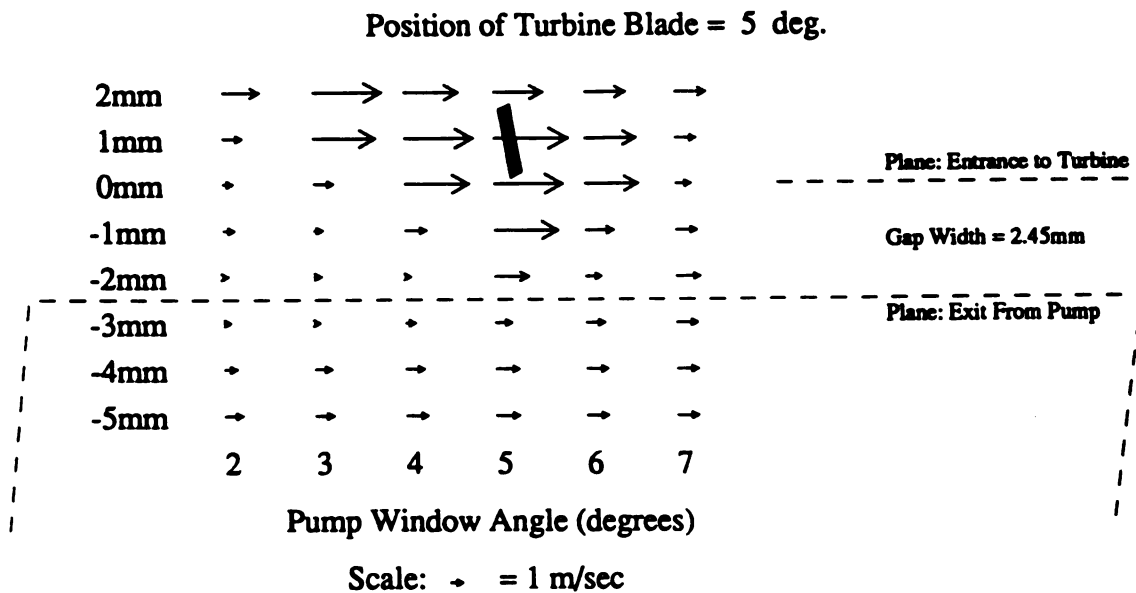
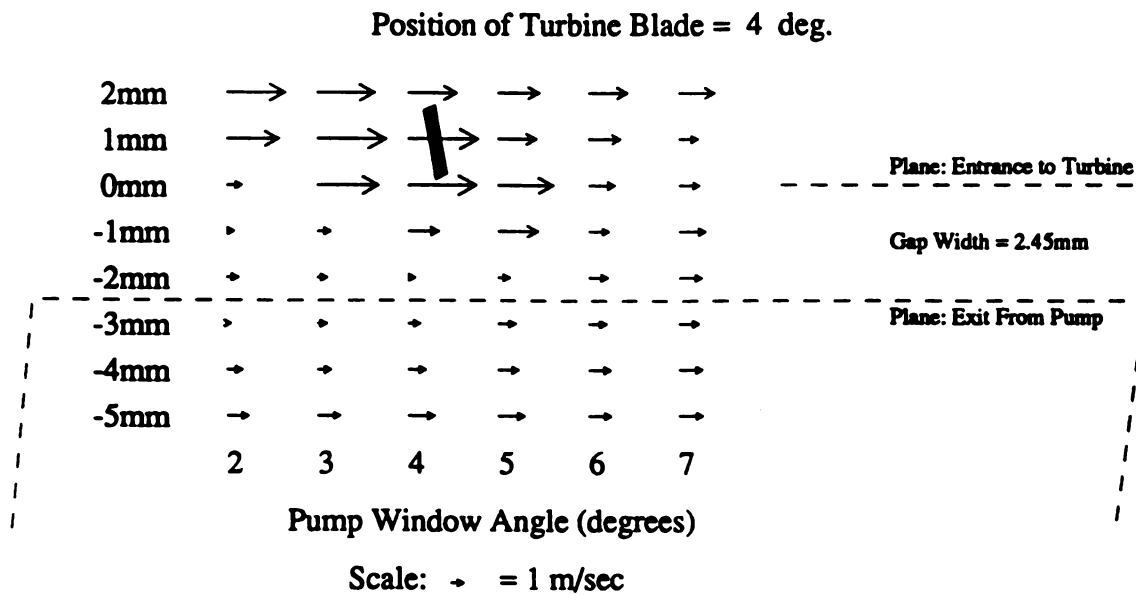


Figure 38. (continued)

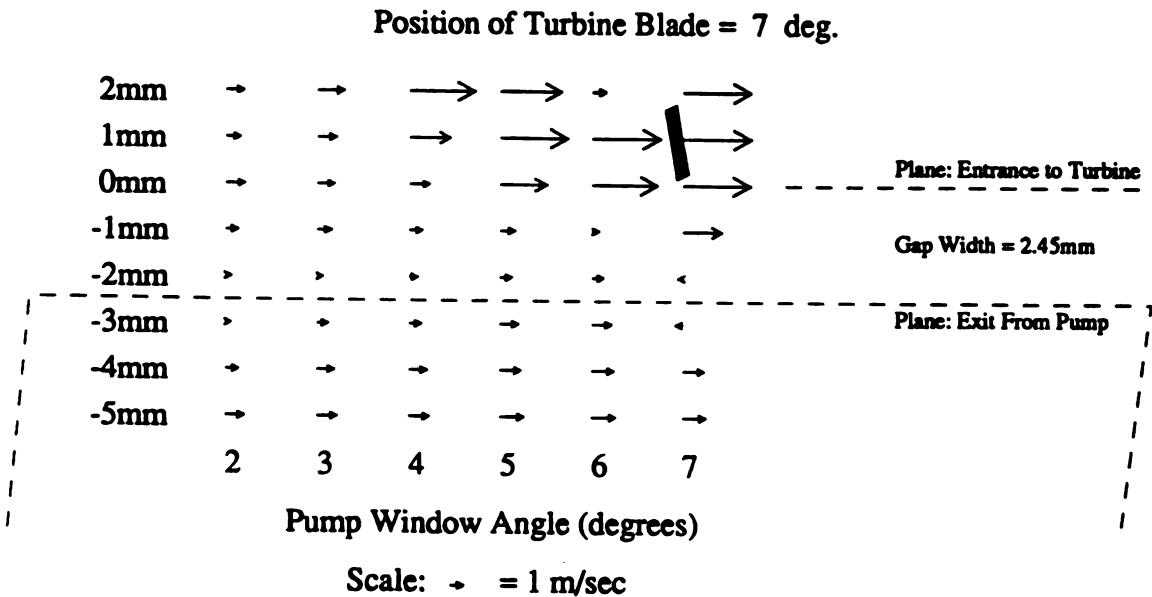
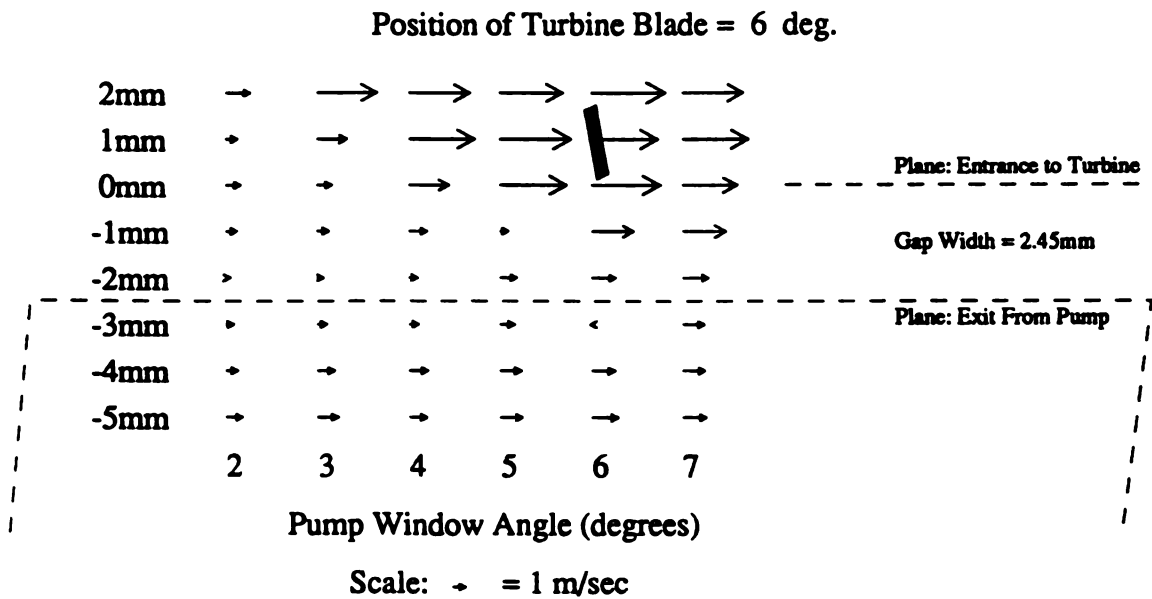
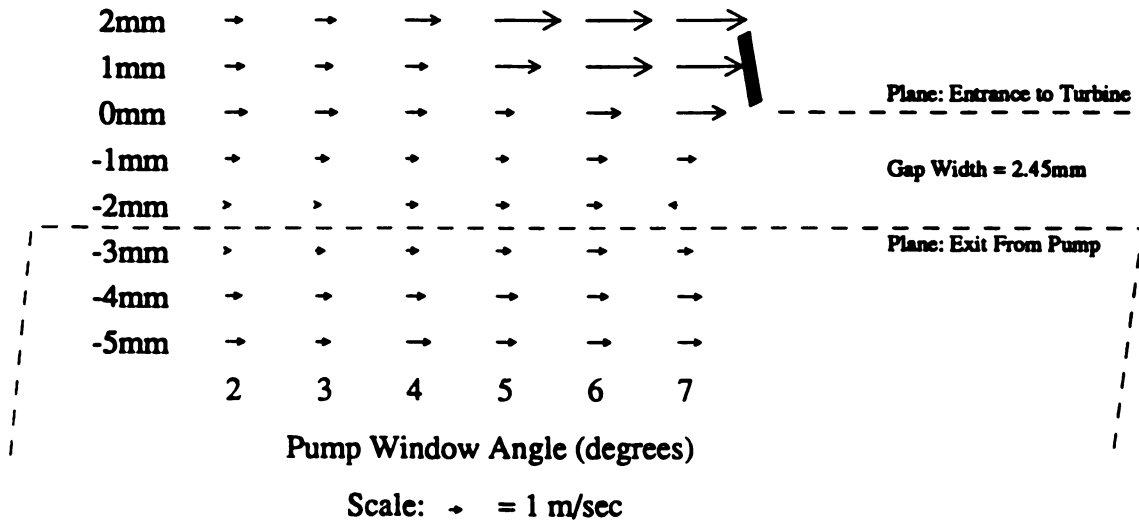


Figure 38. (continued)

Position of Turbine Blade = 8 deg.



Position of Turbine Blade = 9 deg.

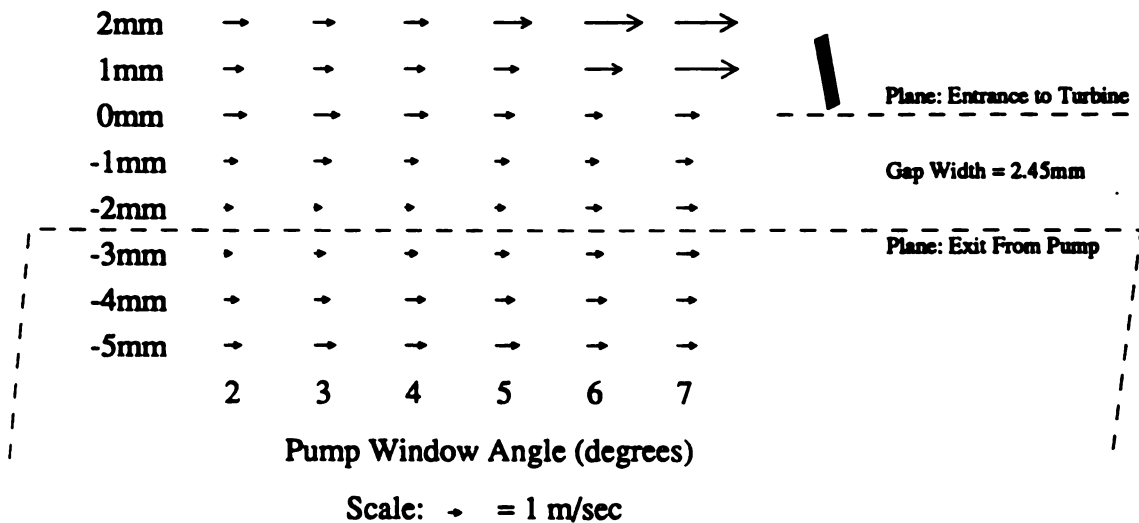
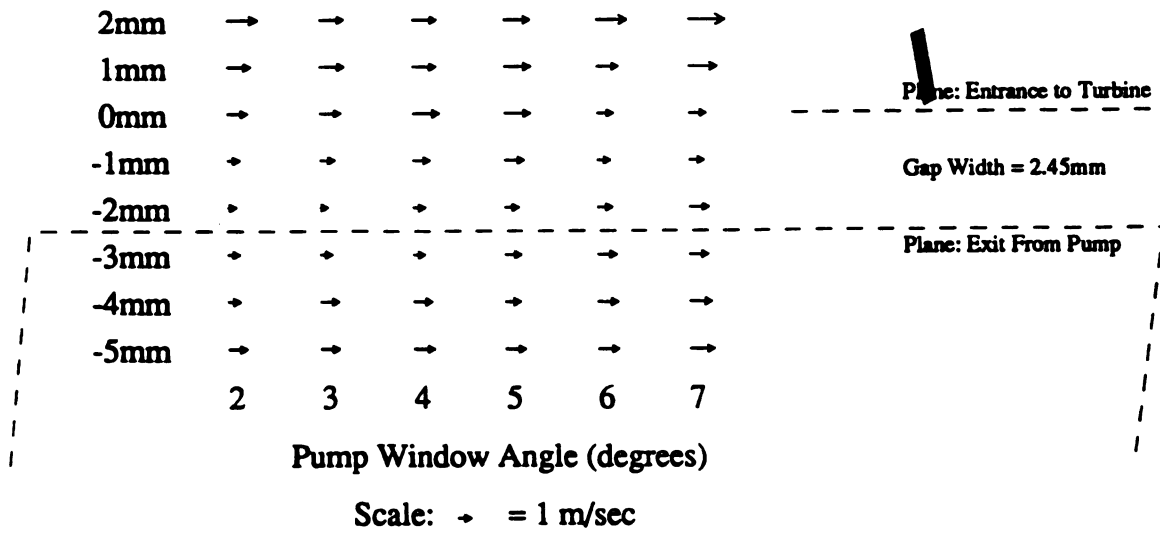


Figure 38. (continued)

Position of Turbine Blade = 10 deg.



Position of Turbine Blade = 11 deg.

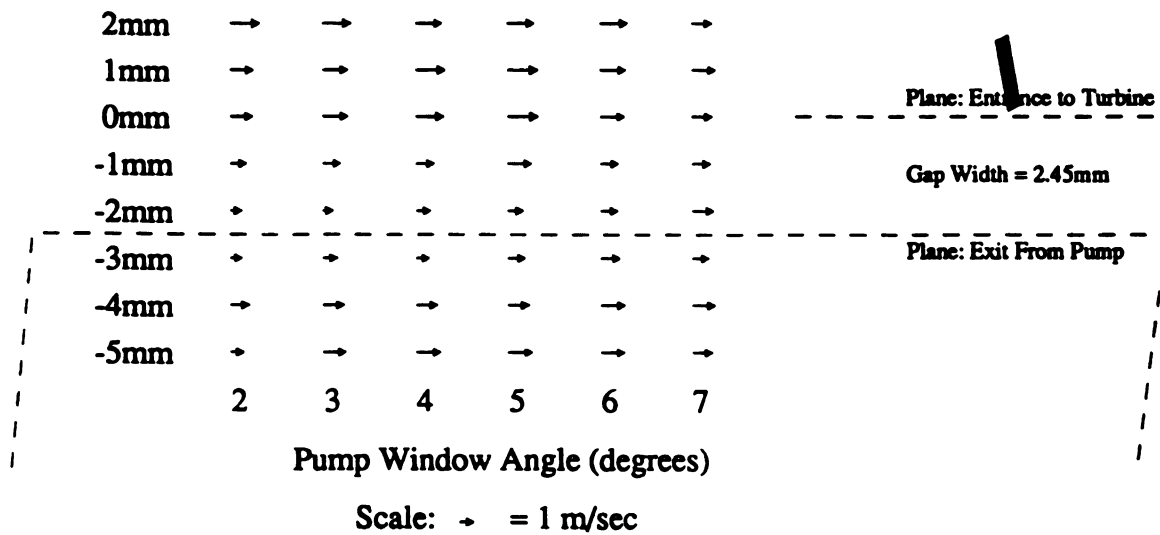
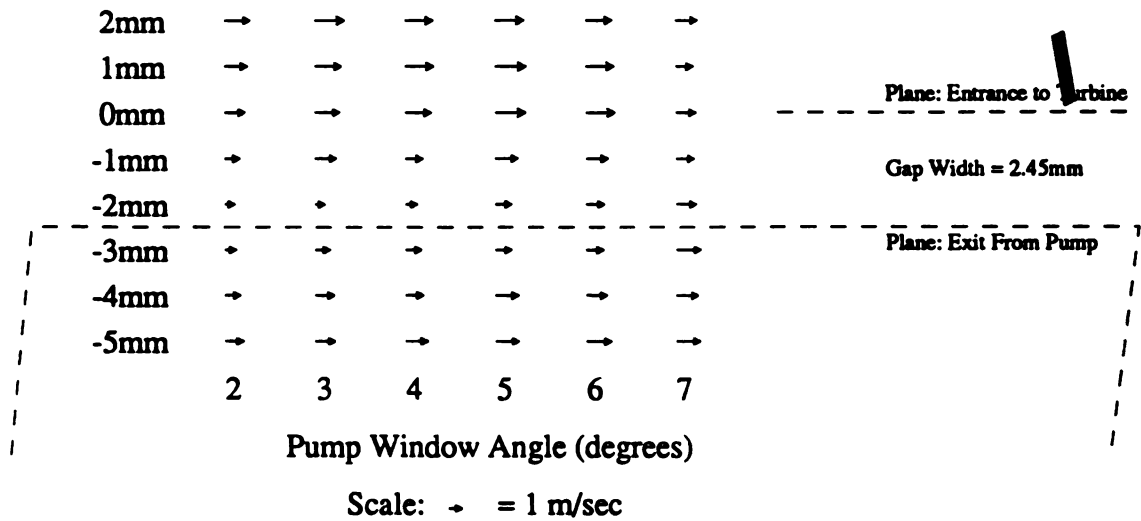


Figure 38. (continued)

Position of Turbine Blade = 12 deg.



Position of Turbine Blade = 13 deg.

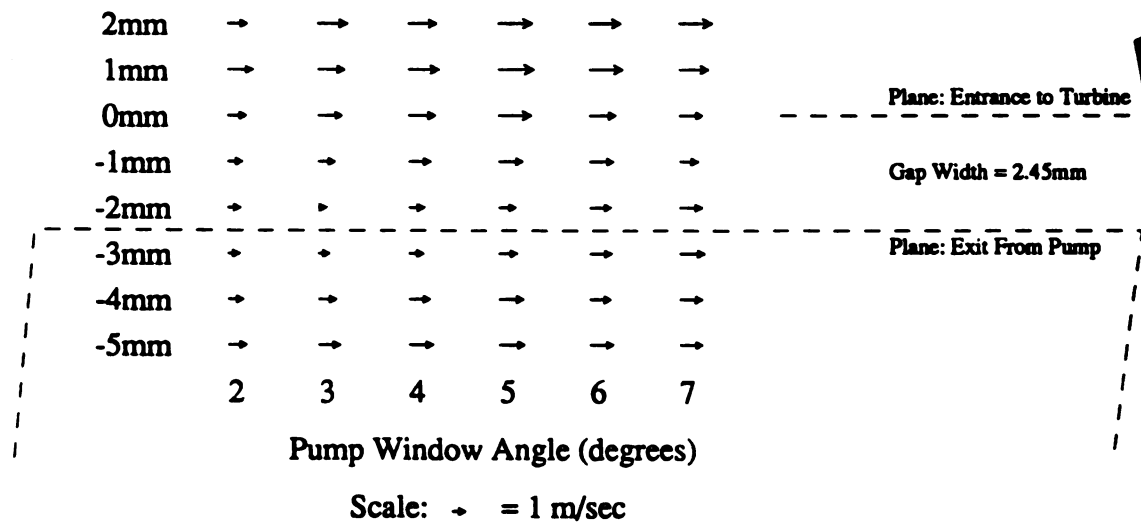


Figure 38. (continued)

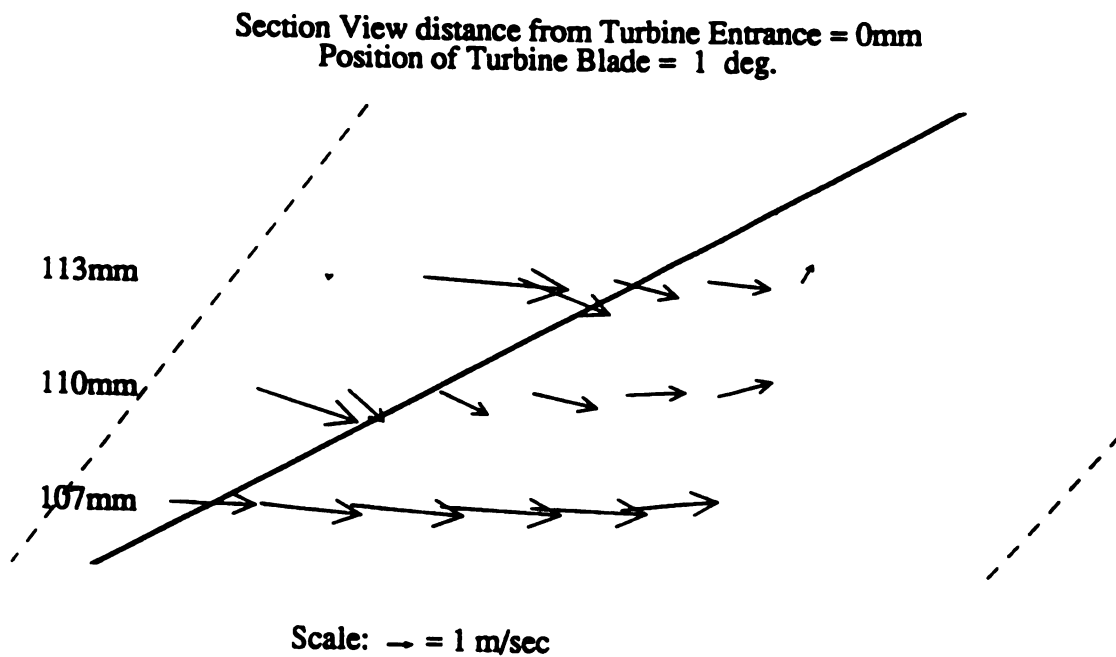
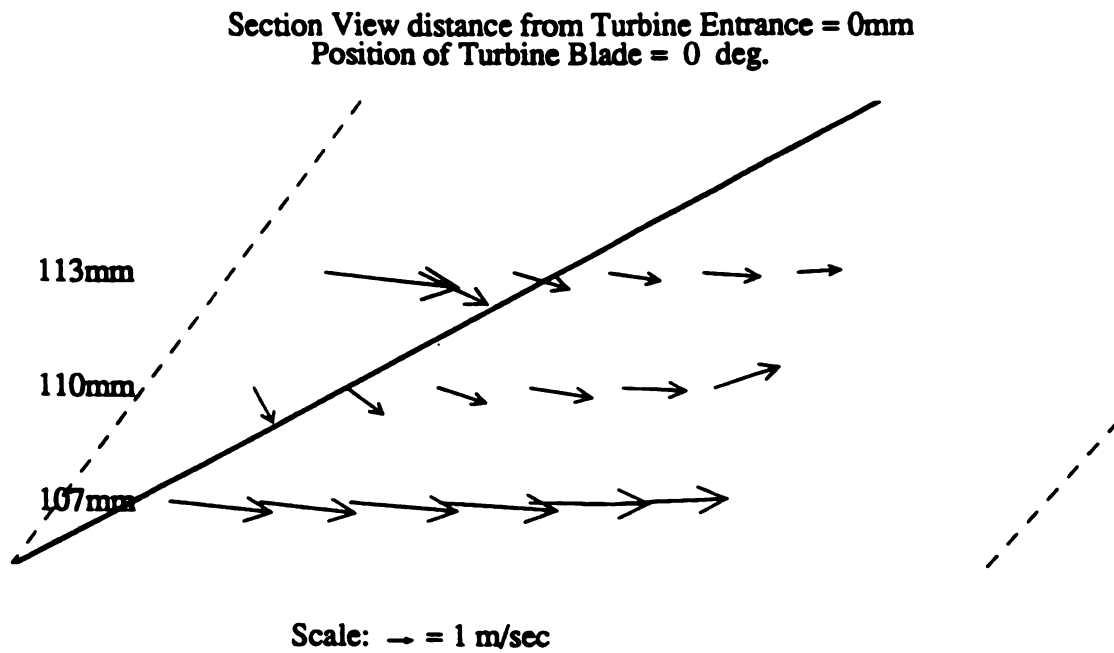


Figure 39. X and Y resultant velocity vectors at turbine entrance

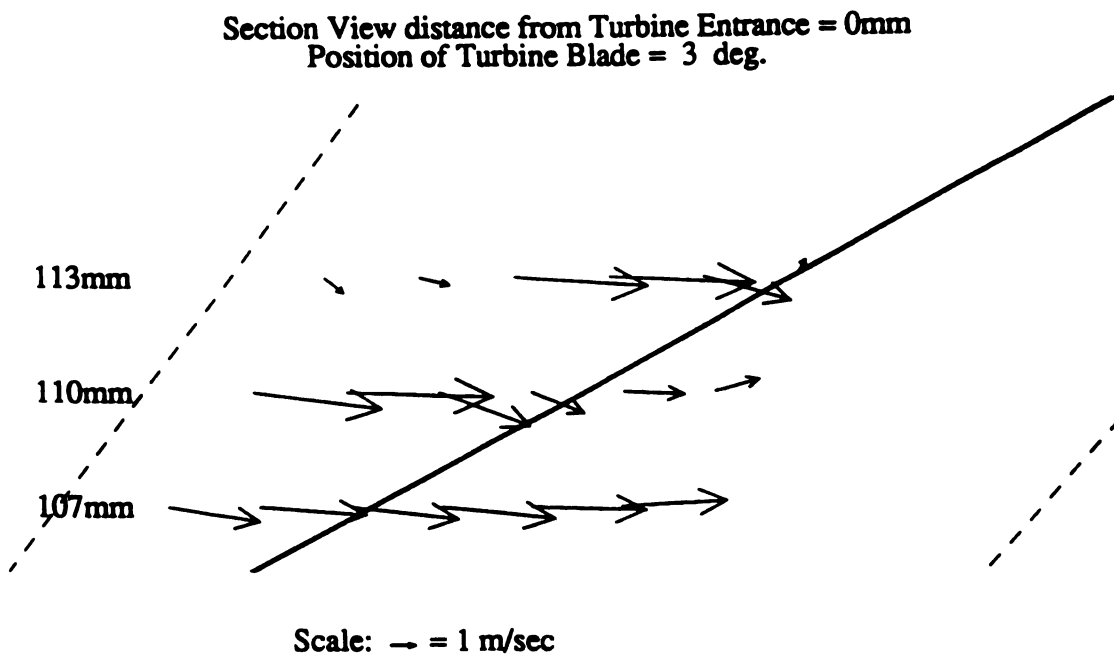
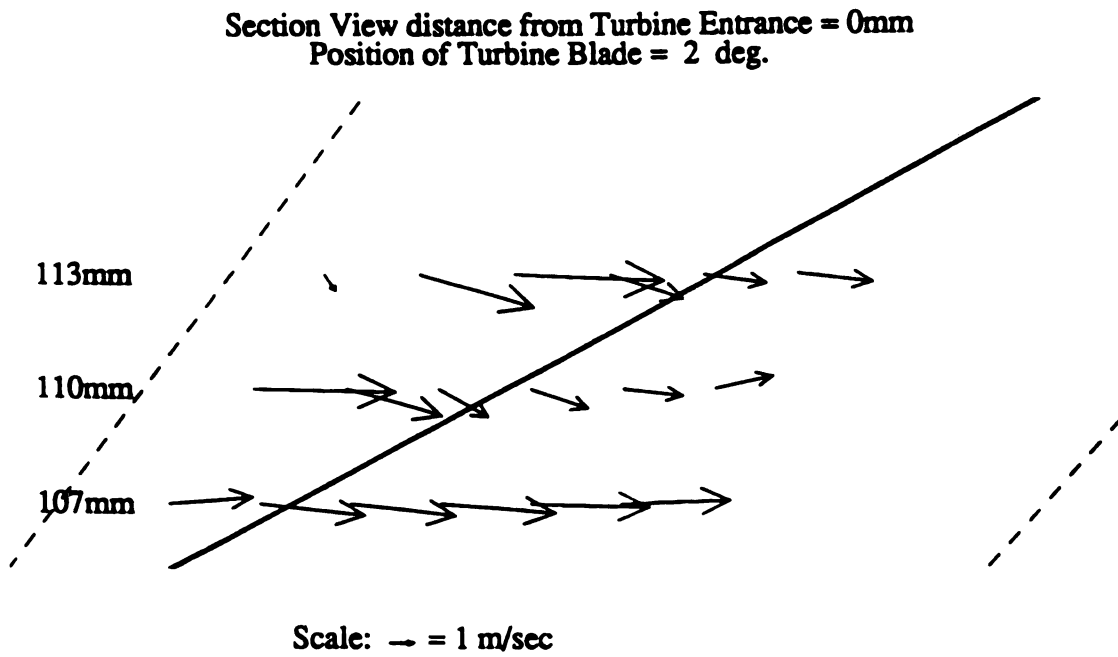
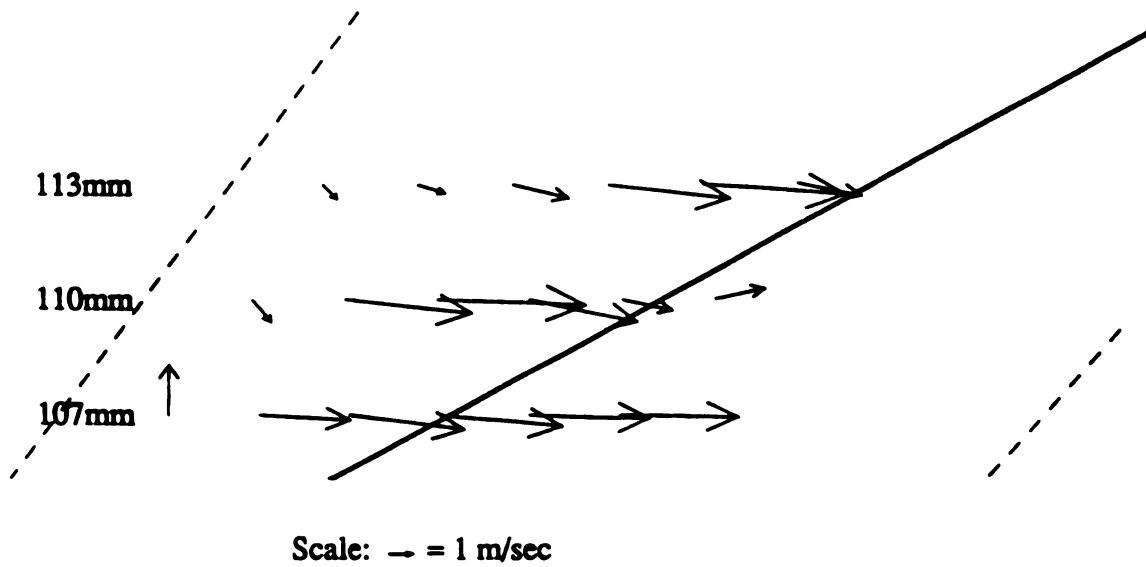


Figure 39. (continued)

Section View distance from Turbine Entrance = 0mm
Position of Turbine Blade = 4 deg.



Section View distance from Turbine Entrance = 0mm
Position of Turbine Blade = 5 deg.

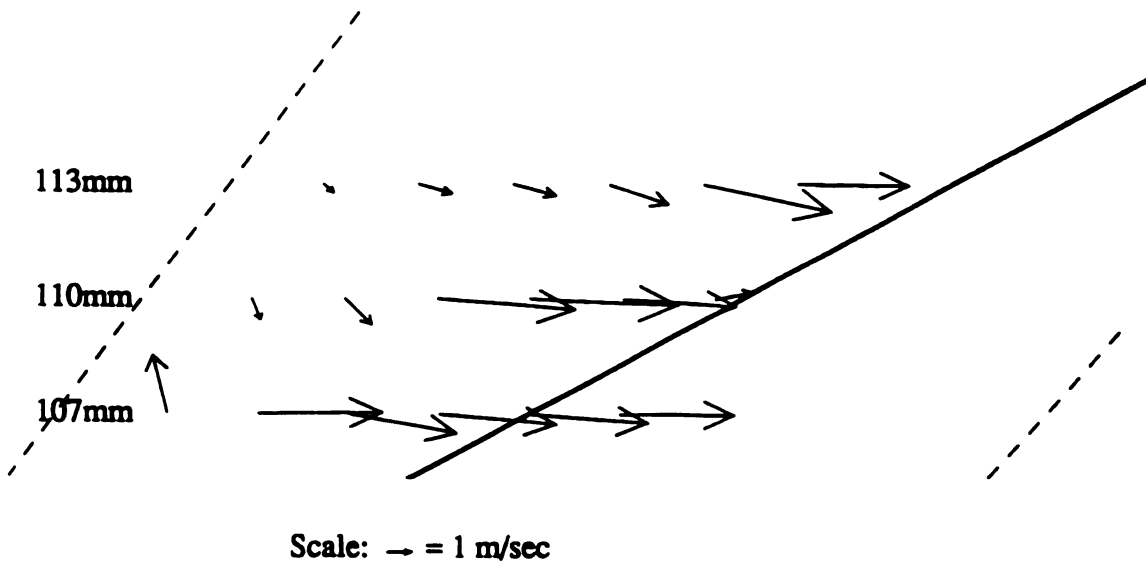
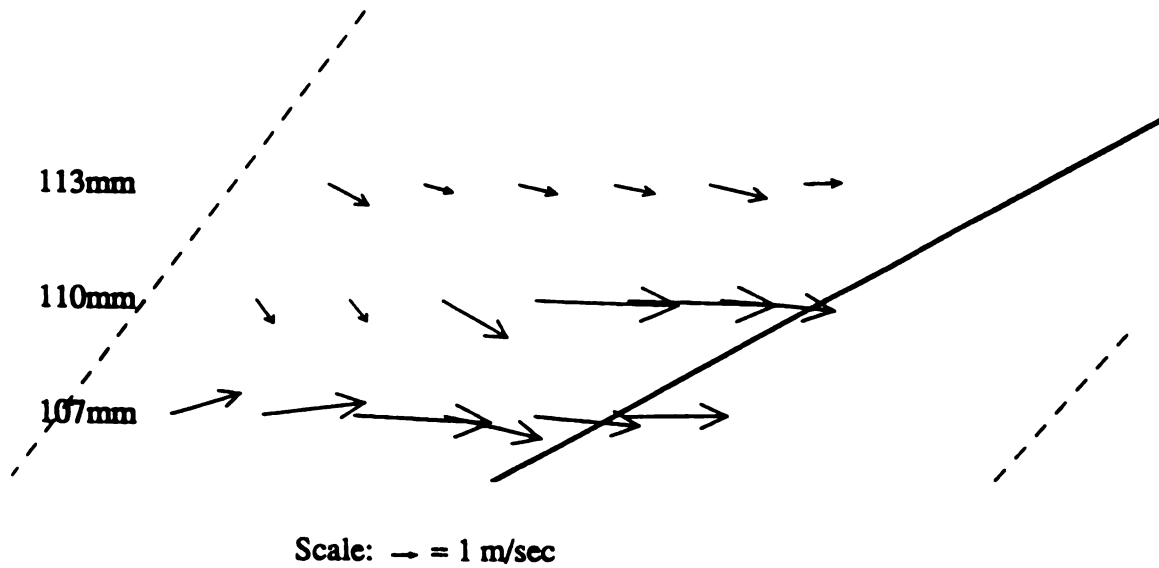


Figure 39. (continued)

Section View distance from Turbine Entrance = 0mm
Position of Turbine Blade = 6 deg.



Section View distance from Turbine Entrance = 0mm
Position of Turbine Blade = 7 deg.

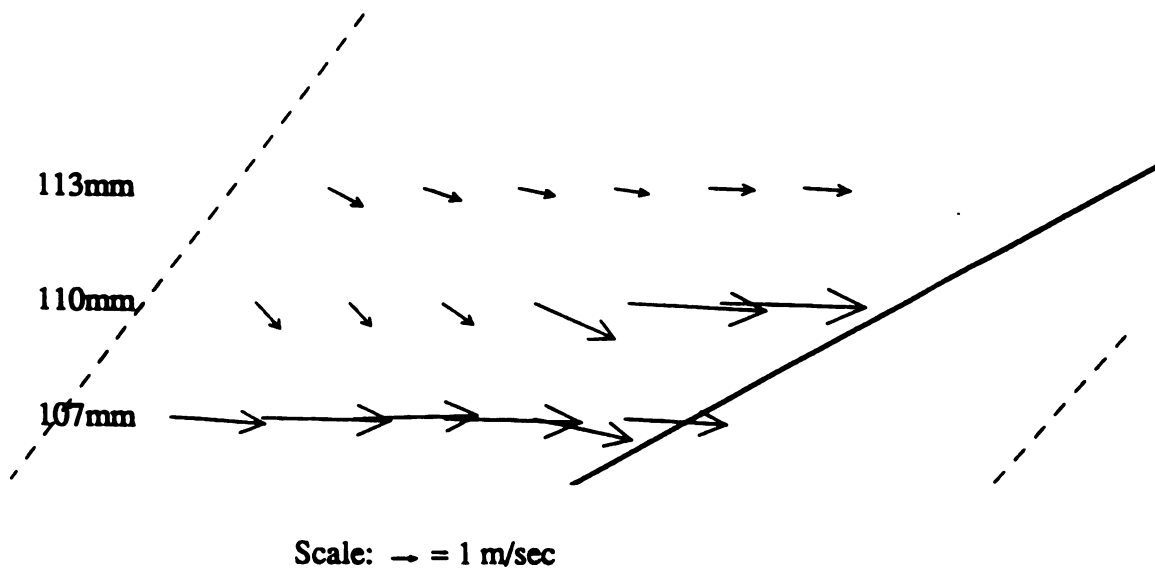
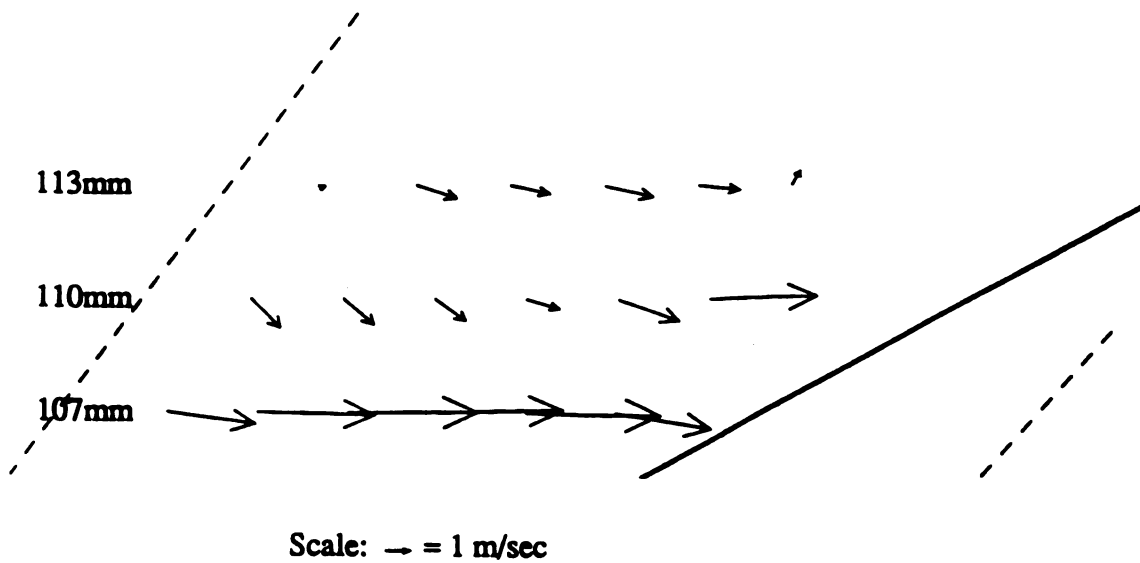


Figure 39. (continued)

Section View distance from Turbine Entrance = 0mm
Position of Turbine Blade = 8 deg.



Section View distance from Turbine Entrance = 0mm
Position of Turbine Blade = 9 deg.

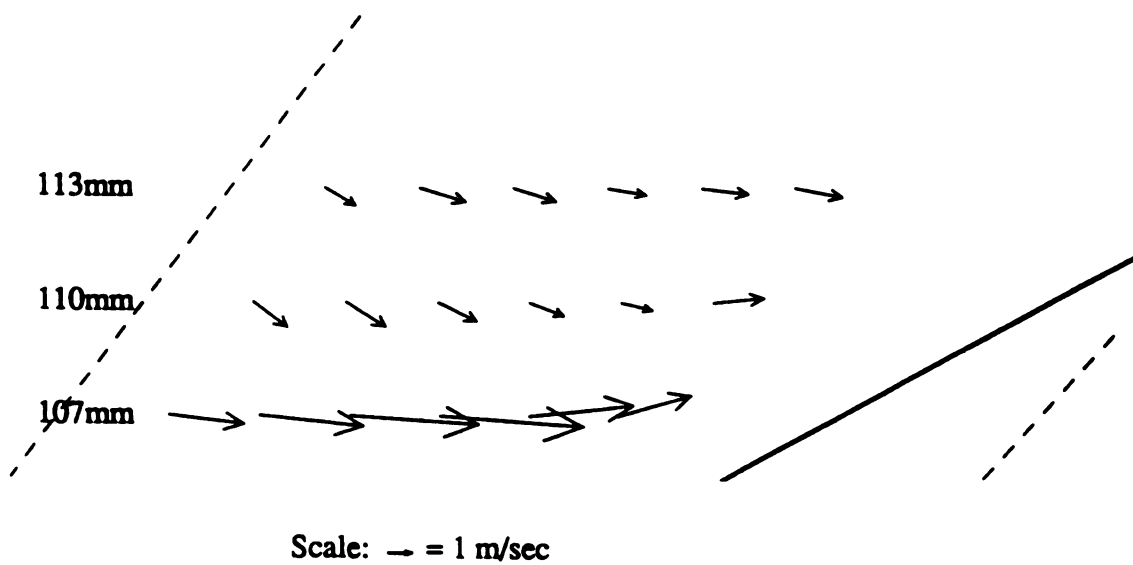
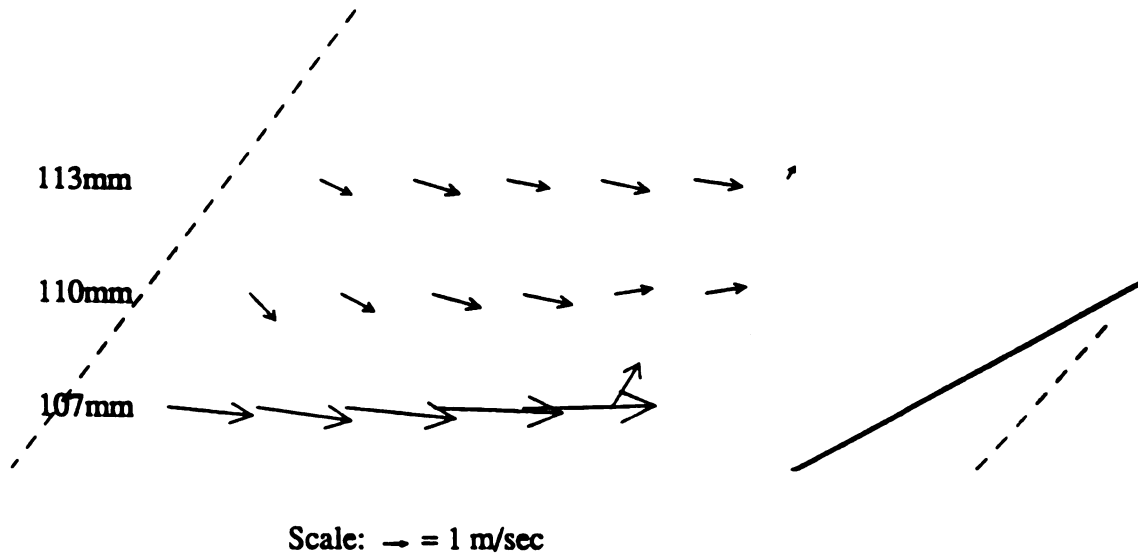


Figure 39. (continued)

Section View distance from Turbine Entrance = 0mm
Position of Turbine Blade = 10 deg.



Section View distance from Turbine Entrance = 0mm
Position of Turbine Blade = 11 deg.

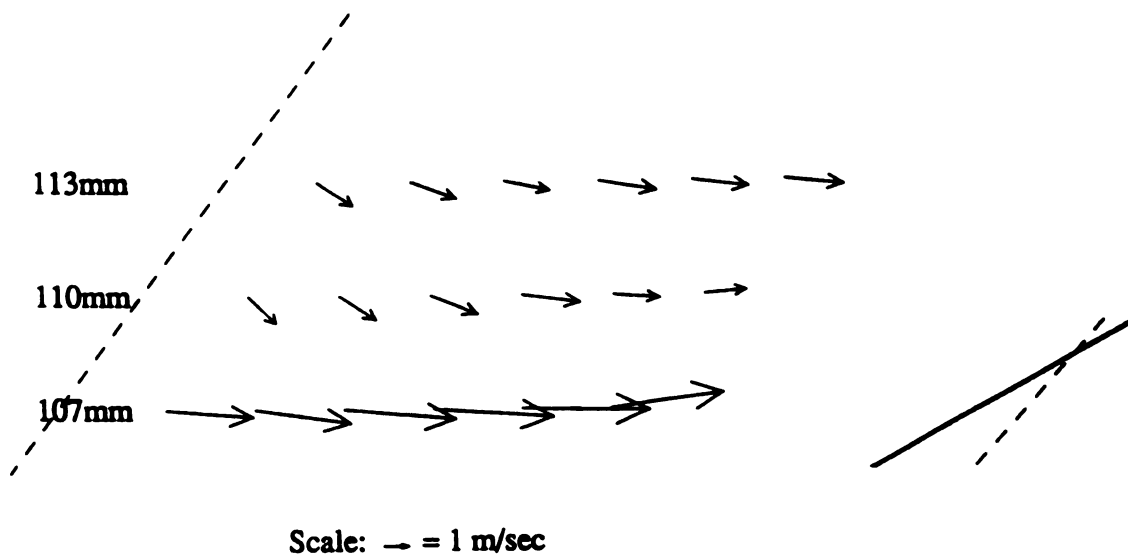


Figure 39. (continued)

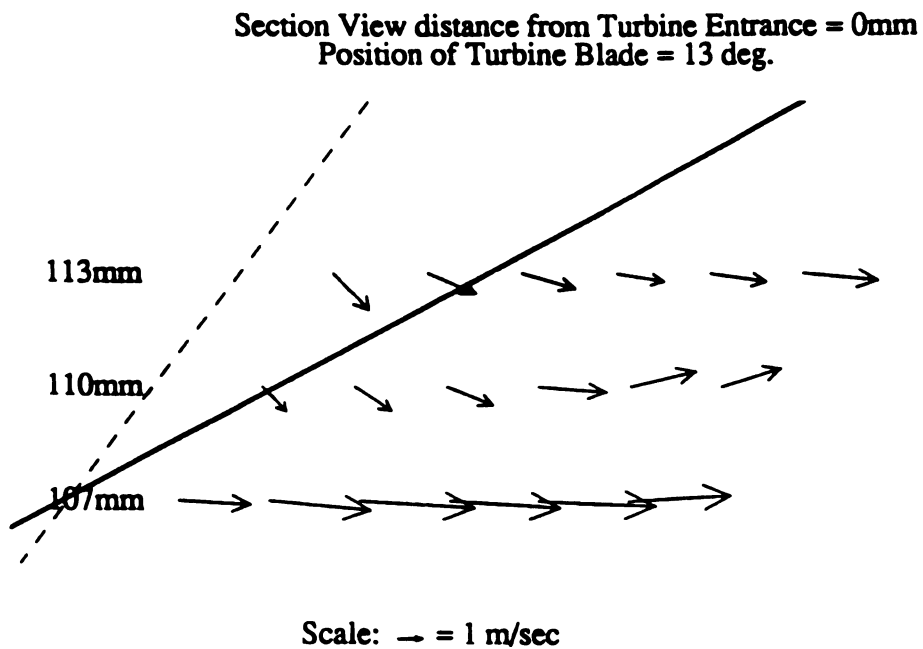
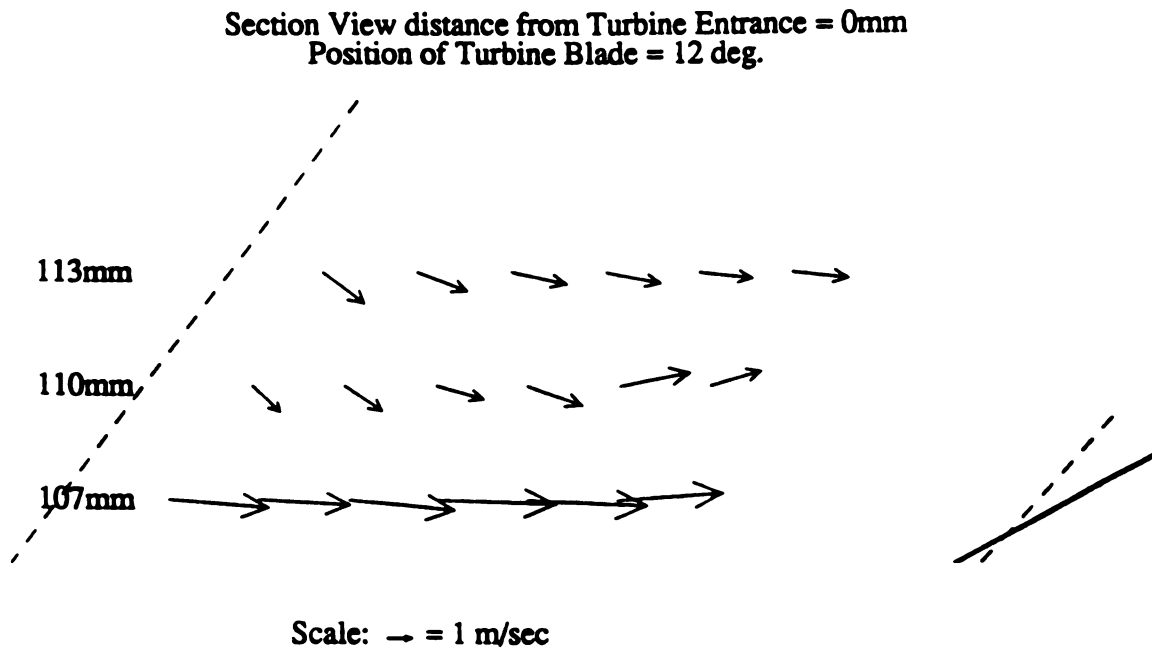


Figure 39. (continued)

CHAPTER 7

SUMMARY AND CONCLUSIONS

In this investigation, a two-component LDV system was used to quantify the flow field in an automotive torque converter. The goal of the study was to determine the feasibility and limitations of the method, and to note any distinct flow characteristics. Measurements were made in two areas of an impeller passage. Due to the limitation of the initial experimental configuration, the first area measured was confined to the middle of the passage and to a depth of 2 mm. Improvements to the experimental configuration expanded the measurement envelope to include the gap region near the impeller and turbine interface. This was the focus of the second area of measurements. Tests were conducted at 1000 and 1500 rpm at four separate speed ratios.

The results of the present study can be summarized as follows:

1. A valid method to obtain information on the flow field inside a torque converter has been developed along with the necessary data processing and presentation techniques. The limitations of this technique appears to be one of optical access for the multiple laser beams.
2. The flow rate inside the impeller passage increases significantly when the speed ratio is decreased from a nearly one-to-one ratio. A further decrease in speed ratio only increases the flow rate slightly and also causes the flow to become more turbulent. The velocity of the flow near the impeller pressure surface is higher than near the suction surface.

3. The instantaneous position of the turbine has little effect on the flow in the impeller passage. The instantaneous position of the turbine does have a noticeable effect on the flow in the gap region between the impeller exit and the turbine entrance.
4. Animations of the velocity vectors near the gap region reveal that the flow in the immediate vicinity of the turbine blade is accelerated as the turbine blade passes by. The flow behind the passing turbine blade is either significantly reduced or reversed. The fluid flow in this area is also more turbulent than the flow elsewhere in the region. This suggests that some type of wake or secondary flow is present behind the turbine blade. Such a secondary flow would result in a loss in converter efficiency. As the turbine blade moves out of the measurement region, the flow tends to settle down and become more steady.
5. Animations also reveal the presence of velocity vectors in the outward radial direction for measurements taken at a radius near the shroud. This suggests that fluid from behind the shroud is reentering the main flow.

CHAPTER 8

RECOMMENDATIONS

In order to continue the progress toward a better understanding of the flow field in an automotive torque converter, the following recommendations for future work seem appropriate.

1. New windows could be fabricated and placed in the converter. Specifically, a window might be placed on the circumference of the converter along the intersection of the impeller exit and turbine entrance. The entire test stand could then be rotated 90° and the existing two-component LDV system could be used to measure the Z velocity component.
2. The possibility of using quartz as a window material needs to be further investigated. Quartz would eliminate the current temperature restriction of the test stand.
3. Different impeller blade shapes could be tested by making a section of impeller blades removable. This technique had already been used in the University of Michigan study.
4. The LDV system must be upgraded so that it can measure all three velocity components simultaneously. Without this improvement, only two-thirds of the necessary information can ever be obtained simultaneously. The third velocity component would enable converter parameters such as flow angle, flow rate, force distribution, and secondary flow to be quantified.

LIST OF REFERENCES

LIST OF REFERENCES

1. Polubinski, A.T., "Torque Converter Balance Investigation VSA Variation Simulation Analysis," Ford Motor Company Torque Converter Lab Publication, 1990.
2. By, R.R. and Mahoney, J.E., "Technology Needs for the Automotive Torque Converter — Part 1: Internal Flow, Blade Design, and Performance," SAE Paper No. 880482, 1988.
3. Schodl, R., "A Laser - Two - Focus (L2F) Velocimeter for Automatic Flow Vector Measurements in the Rotating Components of Turbomachines," Journal of Fluids Engineering, Transactions of the ASME, Vol. 102, No. 4, pp. 412 - 419, 1980.
4. Hayami, H., Senoo, Y. and Ueki H., "Flow in the Inducer of a Centrifugal Compressor Measured With a Laser Velocimeter," Journal of Engineering for Gas Turbines and Power, Transactions of the ASME, Vol. 107, No. 2, pp. 534 - 540, 1985.
5. Flack, R.D., Hamkins, C.P. and Brady D.R., "Laser Velocimeter Turbulence Measurements in Shrouded and Unshrouded Radial Flow Pump Impellers," International Journal of Heat and Fluid Flows, Vol. 8, No. 1, pp. 16 - 25, 1987.
6. Fister, W. and Adrian, F.W., "Experimental Researches of Flow in Hydrodynamic Torque Converters," Proceeding of the 7th Conference of Fluid Machinery in Budapest, Hungary, Vol. 1, pp. 210-224, 1983.
7. Bahr, H.M., Flack, R.D., By, R.R. and Zhang, J.J., "Laser Velocimeter Measurements in the Stator of a Torque Converter," SAE Paper No. 901769, 1990.
8. Numazawa, A., Ushijima, F., Fukumura, K. and Ishihara, T., "An Experimental Analysis of Fluid Flow in a Torque Converter," SAE Paper No. 830571, 1983.

9. Laser Anemometry Theory, Application, & Techniques, A TSI Publication, 1982.
10. Fax transmitted by G.R. Becraft, Ford Motor Company Torque Converter Laboratory, Livonia, Michigan, August 11, 1992.
11. Menon, R. and Lai W.T., "Key Considerations in the Selection of Seed Particles for LDV Measurements," Proceedings of the 4th International Conference on Laser Anemometry in Cleveland, Ohio, 1991.
12. Dring R.P., "Sizing Criteria for Laser Anemometry Particles," Journal of Fluids Engineering, Transactions of ASME, Vol. 104, pp. 15-17, 1982.
13. Schlichting, H., Boundary-Layer Theory, 6th ed., New York: McGraw-Hill Book Company, 1968.

MICHIGAN STATE UNIV. LIBRARIES



31293008812608